2014-06

Ignition delay properties of alternative fuels with Navy-relevant diesel injectors

Rydalch, Andrew J.

Monterey, California: Naval Postgraduate School

NAVAL POSTGRADUATE SCHOOL

MONTEREY, CALIFORNIA

THESIS

IGNITION DELAY PROPERTIES OF ALTERNATIVE FUELS WITH NAVY-RELEVANT DIESEL INJECTORS

by

Andrew J. Rydalch

June 2014

Thesis Advisor:	Christopher M. Brophy
Second Reader:	Sanjeev Sathe

Approved for public release; distribution is unlimited

THIS PAGE INTENTIONALLY LEFT BLANK

REPORT DOCUMENTATION PAGE

Form Approved OMB No. 0704-0188

1. AGENCY USE ONLY ***(Leave blank)***	**2. REPORT DATE** June 2014	**3. REPORT TYPE AND DATES COVERED** Master's Thesis

4. TITLE AND SUBTITLE
IGNITION DELAY PROPERTIES OF ALTERNATIVE FUELS WITH NAVY-RELEVANT DIESEL INJECTORS

5. FUNDING NUMBERS
N0001414WX00788

6. AUTHOR(S) Andrew J. Rydalch

7. PERFORMING ORGANIZATION NAME(S) AND ADDRESS(ES)
Naval Postgraduate School
Monterey, CA 93943-5000

8. PERFORMING ORGANIZATION REPORT NUMBER

9. SPONSORING /MONITORING AGENCY NAME(S) AND ADDRESS(ES)
N/A

10. SPONSORING/MONITORING AGENCY REPORT NUMBER

11. SUPPLEMENTARY NOTES The views expressed in this thesis are those of the author and do not reflect the official policy or position of the Department of Defense or the U.S. Government. IRB Protocol number ____N/A____.

12a. DISTRIBUTION / AVAILABILITY STATEMENT
Approved for public release; distribution is unlimited

12b. DISTRIBUTION CODE

13. ABSTRACT (maximum 200 words)

In support of the Navy's Green Fleet Initiative, this thesis researched the ignition characteristics for diesel replacement fuels used with Navy-relevant fuel injectors. A constant-volume combustion chamber was used to simulate Top-Dead-Center conditions of a diesel engine using an ethylene-air preburn with appropriate make-up oxygen. The injection conditions ranged from temperatures of 1,000 K to 1,300 K and densities has high as 14.8 kg/m^3. Hydrotreated renewable diesel (HRD) and direct sugar-to-hydrocarbon (DSH) fuels were injected into the combustion chamber using a Sturman research injector, a Yanmar injector, and an Electro Motive Diesel (EMD) injector. The primary means of data collection was optical emission imaging of laser induced fluorescence of the fuel and broadband emission of the combustion event. The ignition delay was determined using high speed imaging at 50 kHz to determine the time delay between start of injection and start of combustion. The results of the study show that the ignition delay characteristics for the F-76/HRD 50/50 blend are compatible with those of conventional F-76 diesel fuel for both the Yanmar and EMD injectors at the conditions tested. The ignition delay characteristics of the F-76/DSH 50/50 blend fuel for the Yanmar injector were also compatible with those of F-76.

14. SUBJECT TERMS F-76, HRD, DSH, CVCC, ignition delay, preburn, diesel injector, alternative fuels	**15. NUMBER OF PAGES** 89
	16. PRICE CODE

17. SECURITY CLASSIFICATION OF REPORT	**18. SECURITY CLASSIFICATION OF THIS PAGE**	**19. SECURITY CLASSIFICATION OF ABSTRACT**	**20. LIMITATION OF ABSTRACT**
Unclassified	Unclassified	Unclassified	UU

NSN 7540-01-280-5500

Standard Form 298 (Rev. 2-89)
Prescribed by ANSI Std. 239-18

THIS PAGE INTENTIONALLY LEFT BLANK

Approved for public release; distribution is unlimited

IGNITION DELAY PROPERTIES OF ALTERNATIVE FUELS WITH NAVY-RELEVANT DIESEL INJECTORS

Andrew J. Rydalch
Ensign, United States Navy
B.S., United States Naval Academy, 2013

Submitted in partial fulfillment of the
requirements for the degree of

MASTER OF SCIENCE IN MECHANICAL ENGINEERING

from the

NAVAL POSTGRADUATE SCHOOL
June 2014

Author: Andrew J. Rydalch

Approved by: Christopher M. Brophy
Thesis Advisor

Sanjeev Sathe
Second Reader

Knox T. Millsaps
Chair, Department of Mechanical and Aerospace Engineering

THIS PAGE INTENTIONALLY LEFT BLANK

ABSTRACT

In support of the Navy's Green Fleet Initiative, this thesis researched the ignition characteristics for diesel replacement fuels used with Navy-relevant fuel injectors. A constant-volume combustion chamber was used to simulate Top-Dead-Center conditions of a diesel engine using an ethylene-air preburn with appropriate make-up oxygen. The injection conditions ranged from temperatures of 1,000 K to 1,300 K and densities has high as 14.8 kg/m^3. Hydrotreated renewable diesel (HRD) and direct sugar-to-hydrocarbon (DSH) fuels were injected into the combustion chamber using a Sturman research injector, a Yanmar injector, and an Electro Motive Diesel (EMD) injector. The primary means of data collection was optical emission imaging of laser induced fluorescence of the fuel and broadband emission of the combustion event. The ignition delay was determined using high speed imaging at 50 kHz to determine the time delay between start of injection and start of combustion. The results of the study show that the ignition delay characteristics for the F-76/HRD 50/50 blend are compatible with those of conventional F-76 diesel fuel for both the Yanmar and EMD injectors at the conditions tested. The ignition delay characteristics of the F-76/DSH 50/50 blend fuel for the Yanmar injector were also compatible with those of F-76.

THIS PAGE INTENTIONALLY LEFT BLANK

TABLE OF CONTENTS

LIST OF FIGURES

LIST OF TABLES

THIS PAGE INTENTIONALLY LEFT BLANK

LIST OF ACRONYMS AND ABBREVIATIONS

BD	biodiesel
BDC	Bottom-Dead-Center
BNC	Bayonet Neill-Concelman
CI	compression ignition
CN	Cetane number
CVCC	Constant Volume Combustion Chamber
DI	direct injection
DOD	Department of Defense
DON	Department of the Navy
DSH	Direct Sugar-to-Hydrocarbon
EMD	Electro Motive Diesel
FAO	Food and Agriculture Organization
FT	Fischer-Tropsch
HRD	Hydrotreated Renewable Diesel
HRR	heat-release rate
ID	ignition delay
NPS	Naval Postgraduate School
NATO	North Atlantic Treaty Organization
NAVAIR	Naval Air Systems Command
PFA	perfluoroalkoxy
Re	Reynolds Number
RIMPAC	Rim of the Pacific
SOC	start of combustion
SOI	start of injection
SPK	Synthetic Paraffinic Kerosene
STP	Standard Temperature and Pressure
TDC	Top-Dead-Center
We	Weber Number

THIS PAGE INTENTIONALLY LEFT BLANK

ACKNOWLEDGMENTS

I would like to thank Dr. Chris Brophy for his guidance and mentorship throughout the entire research process. His overall vision and depth of understanding for the project were invaluable.

I would also like to thank Dr. Sanjeev Sathe for fulfilling the role of second reader for this project. His expertise and understanding of engineering processes were a great help for this thesis.

I would also like to thank Dave Dausen for guidance on the technical aspects of the project. From introducing me to the testing apparatus to advising me on which direction to take in my research, his advice helped me to not only get the project off to a good start, but also enabled a strong.

Additional thanks goes to Bobby Wright for his help with the physical modifications of the testing apparatus. His skill in the shop and attention to detail saved me countless hours of frustration.

Thanks to the Office of Naval Research and Dr. Sharon Beermann Curtin for funding this research.

THIS PAGE INTENTIONALLY LEFT BLANK

I. INTRODUCTION

A. THE GREEN FLEET INITIATIVE

1. Motivation

Consuming 300,000 barrels per day, the Department of Defense (DOD) is the largest consumer of energy in the United States, making up 2% of the total American oil consumption [1]. The U.S. Navy is responsible for using over 25% of that figure, and in fiscal year 2008, the Navy consumed approximately 38.5 million barrels of fuel [1]. Because the U.S. purchases its oil on the open market, fluctuations in oil prices significantly affect the Navy's budget. In the space of one year, the Navy's fuel cost increased from $1.2 billion to $5 billion [1], evidencing the budgeting instability caused by the fluctuating market and the U.S.'s demand for oil being dependent on foreign nations. In 2012, 40% of the petroleum consumed in the U.S. was imported from foreign countries [2]. President Barack Obama and Secretary of Defense Robert Gates have stated that the Unites States' dependence for oil on foreign countries that are not allies is an issue of national security [3].

In October 2009, the secretary of the Navy, the Honorable Ray Mabus, outlined the future of the U.S. Navy's energy use [4]. Citing concerns of the aforementioned vulnerability in the country's energy and national security, as well as concerns over the harmful effects oil use has on the environment, Mabus outlined five energy targets that the Department of the Navy (DON) would meet over the next 10 years. These targets have become to be known as the Navy's "Green Fleet Initiative." Each of these targets centers upon fiscal and environmental improvements that would help resolve the Navy's energy concerns. The secretary stated the goal for the "Great Green Fleet" composed entirely of ships and aircraft fueled solely from alternative sources of energy and discussed the development of new classes of combatant ships running on hybrid electric alternative power systems. Iconically, Mabus stated that the Navy plans to shift its current alternative energy usage from 17% to 50% of its total power generation. Of the

five energy targets given, three deal directly with shifting energy use from petroleum fuels to alternative fuels [4].

In order to accomplish this shift to alternative forms of energy production, the Navy is interested in the effects of switching its current platforms, designed to be fueled by F-76 Marine Grade Diesel, to alternative fuels. The Navy is searching for a direct drop-in alternative fuel that can replace the conventional, petroleum based fuel. A drop-in fuel is "any fuel that can be used in place of its petroleum counterpart without requiring any modifications to the fuel tank, fuel system, or engine components" [5]. Essentially, the fuel must "look, smell, and taste the same" [6]. Because of the Navy's mission, it is critical that the switch to alternative fuels does not degrade the combat capabilities of the affected platforms. An effective drop-in replacement fuel would have instant benefits without incurring additional costs.

2. Alternative Fuel Qualification

Figure 1 shows the fuel qualification process that is used by the Navy. This process has been developed to determine whether or not a specific biofuel will be compatible for drop-in replacement for petroleum-based Navy platforms. Rick Kamin, the Navy's Fuels Team lead for aircraft at Naval Air Systems Command (NAVAIR) described the qualification process steps as:

> We look at the specification properties that we currently buy fuel to, and that's the first step of the testing – does it meet the current specification properties? Then with success in that, we move to what we call the 'fit for purpose' properties … those things that we don't typically measure in the specification but are critical for performance in an aircraft or ship. "Then we move on to the component testing ... We do component and rig testing to make sure that the performance of the hardware is the same with these fuels [7].

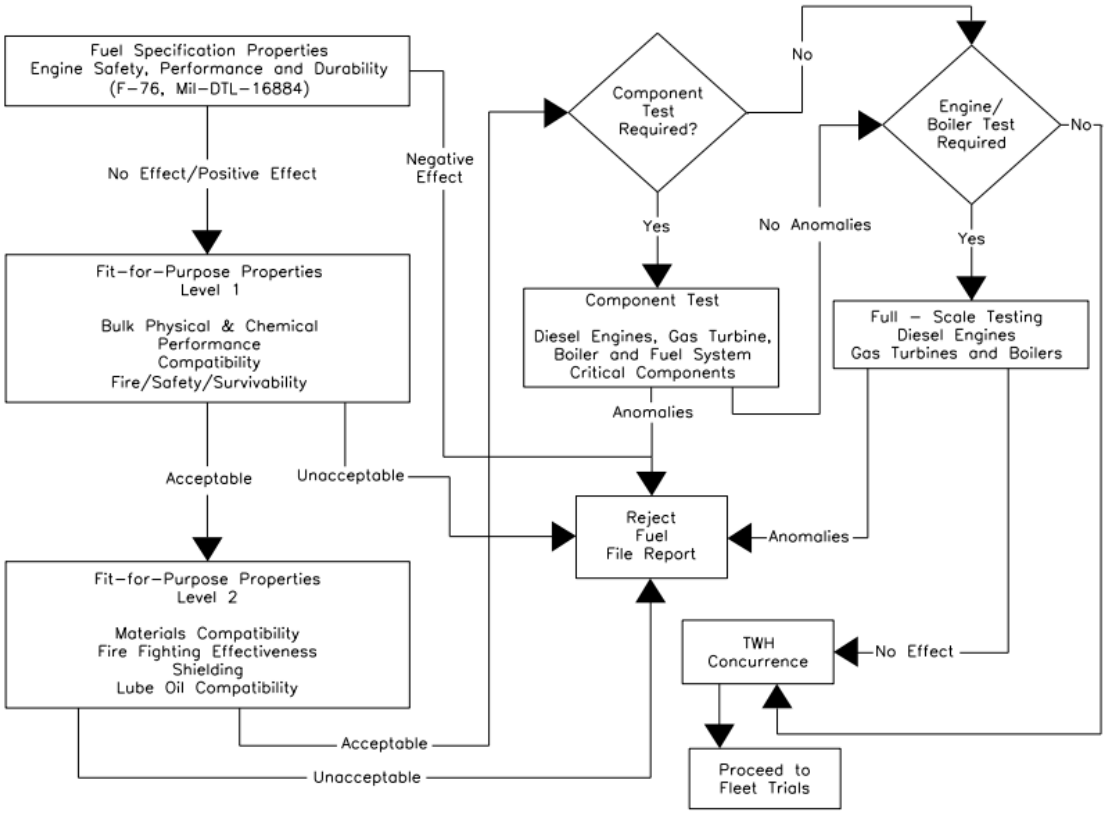

Figure 1 Navy fuel qualification process, from [5].

Because of the rigorous qualification standards, in the five years since the Navy's announcement of its intentions concerning alternative fuels, no fuel has yet been fully qualified for ship implementation [5]. The Navy is examining a broad spectrum of biofuels, including Biodiesel (BD), Fischer-Tropsch (FT), Synthetic Paraffinic Kerosene (SPK), Hydrotreated Renewable Diesel (HRD), and Direct Sugar-to-Hydrocarbon fuels (DSH) [8]. The fuel specification properties for each of these fuels are shown in Table 1.

Fuel / Properties	F-76	BD	FT	HRD	SPK|	DSH
ρ [kg/m^3]	844.2 [a]	885.1	753.9 [a]	778.1 [a]	740	766 [a]
σ [mN/m]	25.8 [b]	24.0	25.3	24.9 [b]	26.8	26
μ (cSt)	2.955 [c]	6.489	4.503	2.748 [c]	1.088 [c]	4.1 [a]
T_{10} -T_{90} [°C]	-	-	173-244	-	-	244-245
T_{50} [°C]	-	-	207.5	-	-	245
LHV [MJ/kg]	42.75	37.6	43.94	43.96	44.05	43.9
Cetane No.	52	56	75	~75	24.7	60
Composition						
Wt% C	86.4	-	96.78	85	84.8	85.1
Wt% H	13.32	-	3.22	15	15.2	14.9
Wt% O	0	10.9	0	0	0	0
% paraffin	70.7	-	95.3	98.5	94.3	99.9
% olefin	2.3	-	1.1	0.9	4.7	0
% aromatic	27	-	3.6	0.6	1.0	0

Table 1 Comparison of biofuel properties at 68 F. [a]Property found at 59 F. [b]Property found at 76 F. [c]Property found at 104 F, from [8].

3. Test Fuels

a. Algae-Based Hydrotreated Renewable Diesel

Traditionally, the term hydrotreated renewable diesel, or HRD, fuel has included alternative fuels derived from hydrocarbon feedstocks of biological origin, such as rapeseed, sunflower, soybean, and palm oil, vegetable oil, and animal fats [8]. Of

particular interest in the field of HRD production is microalgae [9]. Algae-based fuels are referred to as "second-generation" renewable fuels, or "advanced" biofuels because they are produced from non-food biomass; therefore, cultivation of the microalgae does not interfere, either with land or resources, with the production of food [10]. Oil from microalgae is converted to diesel fuel through hydrotreatment, which is a "chemical process where the algal oil reacts with hot pressurized hydrogen gas in the presence of catalysts to remove oxygen-containing functional groups and to hydrogenate unsaturated olefinic compounds" [10]. A study published by the Food and Agriculture Organization of the United Nations (FAO) shows that the hydrotreatment of particular algae can produce an oil yield of 46.7 wt.% [11]. Because of its relatively quick growth and efficient conversion to synthetic diesel fuel, algae derived biofuels are a significant source of energy that can be used in the future [10],[11].

Considering all of the alternative fuels being researched as part of the Green Fleet Initiative, the algae-based HRD is closest to reaching implementation in the fleet [10]. A 50/50 volume blend of this HRD biofuel and conventional NATO F-76 fuel has successfully completed the specification process and is undergoing component testing and field testing. In the summer of 2012, the Navy successfully conducted the Rim of the Pacific (RIMPAC) exercises in which five of the participating ships were powered using a 50/50 blend of F-76 and HRD [12]. This fuel was selected for the particular component testing conducted in this study. Throughout this thesis, the term HRD is referring to the synthetic diesel fuel derived from microalgae. An exhaustive list of the properties of HRD can be found in Hsieh et al. [10].

b. Direct Sugar-to-Hydrocarbon Fuel

As the name implies, the Direct Sugar-to-Hydrocarbon (DSH) fuel process is centered on converting sugars to hydrocarbons. This process is accomplished using a bacterium that consumes the sugar, the source of which can vary. One method has been developed using corn stover: the residue of a corn harvest, including the stalk, leaf, husk, and cob [13]. The sugars from the corn stover act as both the carbon source for the hydrocarbon production and the fuel source for the microbial metabolism. The

hydrocarbon products can be upgraded at small cost to form longer chains that result in the final fuel blendstock [14]. Researchers have been able to achieve successful sugar to hydrocarbon conversion rates on the order of 38%[8]. Similar to the HRD fuel being considered by the Navy, a 50/50 blend of DSH fuel and NATO F-76 fuel is being tested by the navy. This blend was selected for the component testing conducted in this study.

4. Component Testing

For the two fuels discussed above, HRD and DSH, the Navy has enough evidence from the specification and fit-for-purpose studies to move on to direct component testing. The objective of this stage of research is to determine the performance of the new fuel, in a controlled environment without endangering Navy personnel and property.

a. Yanmar Injector

The injector from the Yanmar, 6LPA-STP DI, I-6, 4.16 L engine was selected for this study. This engine is typically found on special warfare boats in the Navy. An image of the Yanmar injector is shown in Figure 2. Essentially, the injector is a spring-loaded needle valve. High-pressure fuel enters the injector and, once the cracking pressure of approximately 3,500 psi is reached, compresses a spring, which opens the valve and sprays high-pressure fuel out of the tip of the injector.

Figure 2 Yanmar injector image.

b. EMD Injector

The Electro Motive Diesel (EMD) 645-E5 DI injector used on a V-16, 169 L engine was also selected for component testing. These diesel engines are used on aircraft carriers throughout the Navy as backup power generators. A cross section diagram of the EMD injector is shown in Figure 3. Fuel is supplied to the injector at a nominal pressure of 60 psi. A hydraulic piston compresses the injector spring, which pressurizes the fuel. Similar to the Yanmar injector, fuel is injected into the chamber via a high pressure nozzle tip.

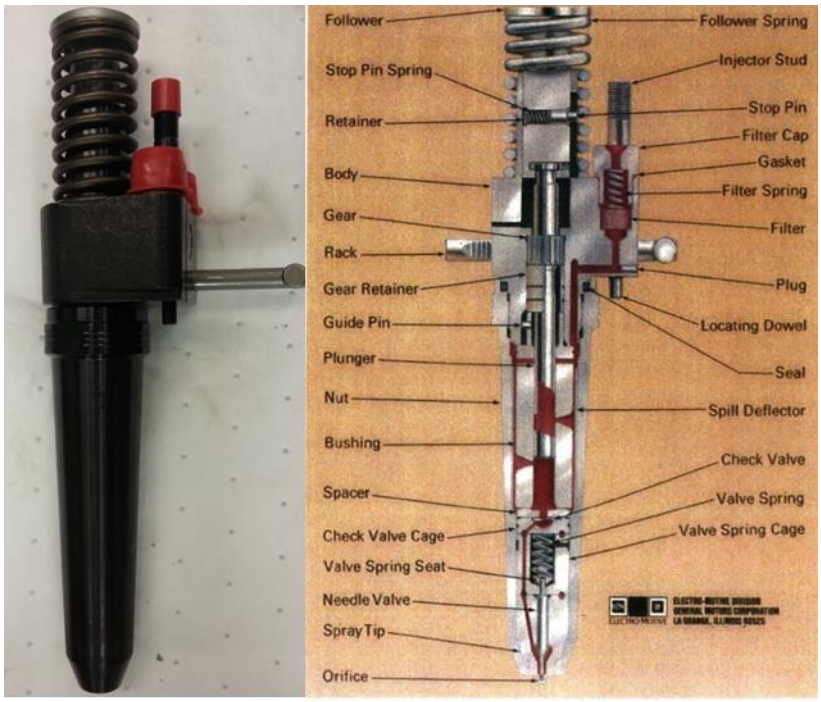

Figure 3 EMD injector cross-sectional view, after [15].

c. Sturman Injector

A Sturman research diesel injector was used to validate the testing set up. This is a research injector that has been used often at the NPS Rocket Lab. The fuel in the injector is supplied at approximately 200 psi and undergoes a 6:1 hydraulic compression before being injected into the chamber at approximately 18,000 psi. The Sturman injector is shown in Figure 4. The injector tip has a single pin which causes the fuel to spray in a hollow cone.

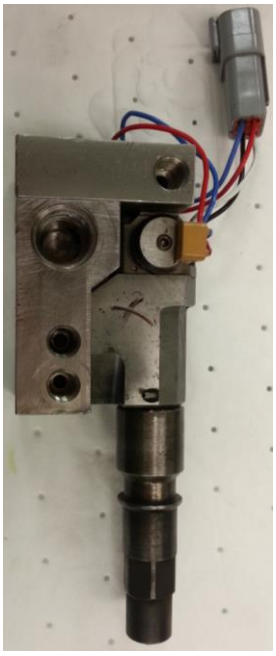

Figure 4 Sturman injector

B. THE DIESEL ENGINE

1. The Diesel Cycle

A typical diesel engine runs a cycle composed of four strokes of a piston. The number of pistons in the engine depends on the size of the engine and the desired power. Figure 5 shows the typical operation of a piston in a diesel engine. The typical engine cycle is composed of four strokes, shown in the figure, and is driven by a crankshaft. The piston is attached to the crankshaft and the lateral translations of the piston are converted into circular rotations of the crankshaft. The cylinder exhaust and filling operations are controlled by a cam shaft.

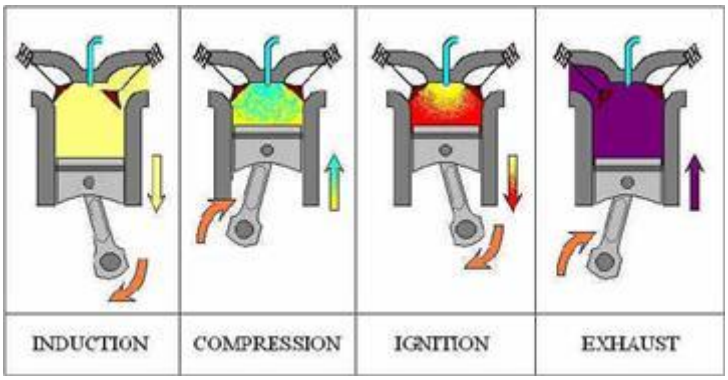

Figure 5 Diesel engine stroke, after [16].

As shown in Figure 5, the piston begins traveling downward from Top-Dead-Center (TDC) and moves to Bottom-Dead-Center (BDC) while the intake valve is open. This represents the first stroke of the cycle, the Induction stroke. The second stroke begins as the intake valve closes and the piston moves from BDC back to TDC. The air in the chamber is volumetrically compressed, typically ranging from a ratio of 11:1 for the smaller diesel engines and 20:1 on the larger engines. This stroke results in a high temperature, and high pressure environment due to the volumetric compression. The ignition or power stroke begins when the injector sprays fuel into the chamber. The high pressure, high temperature environment causes the fuel to combust, which results in even higher temperatures and pressures, and physically pushes the piston down. The fourth stroke, the Exhaust stroke, begins when the piston reaches BDC and the exhaust valve opens, ejecting the hot combustion products from the chamber. When the piston reaches TDC, the Induction stroke begins again and the cycle repeats. It is critical to note that the entire process is driven by the power stroke. The energy introduced into the system in the Power stroke is converted to rotational energy in the crankshaft which drives the other three strokes and provides excess power which can then be extracted from the system.

2. Diesel Cycle Efficiency

Because the diesel cycle is a real-world process, many different factors affect the performance of a diesel engine. From a thermodynamic perspective, the efficiency of the engine is related to the thermal efficiency of its cycle analysis, defined to be the ratio of net work from the cycle and heat added to the cycle. In theory, the network from the

cycle is determined from the relationship between the pressure and volume in the cylinder and is dependent on the position of the piston. The heat addition in a cycle analysis results from the combustion of the injected fuel, increasing the temperature of the already hot, compressed air at TDC. In theory, the efficiency of the process could be improved by increasing the compression ratio, increasing the amount of work available, or decreasing the heat addition; however, these solutions are not always feasible in reality. The compression ratio of an engine is a physical parameter, dependent on chamber and piston size and once past the design phase, the compression ratio cannot be changed for a specific engine. Improving the operating efficiency of existing diesel engines is restricted to adjusting the timing of the fuel injection and properties of the specific fuel used in the engine.

3. Cycle Efficiency Improvements

a. Physical Properties

One of the most critical parameters in diesel engine efficiency is the compression ratio. This ratio largely determines the amount of work that can be produced by the system. Equation (1) shows the relationship between the cycle efficiency, η, and the compression ratio, r [17]. As the compression ratio increases, its inverse decreases and thus the overall efficiency for the cycle increases.

$$\eta \propto 1 - \frac{1}{r} \tag{1}$$

As mentioned previously, the diesel cycle uses volumetric compression, and the compression ratio of a specific engine is a geometry-based parameter dependent on the physical size of the chamber the piston in the engine. Once built, the compression ratio of the chamber cannot be improved over the original design without significant engine modifications. Throughout the lifetime of an engine, the compression ratio can be maintained by proper engine operation, maintenance, and servicing, but can never be improved over the original design value. Because of this relationship, the compression ratio cannot improve the actual operating efficiency of a given engine.

b. Fuel Properties

All of the energy generated in the power stroke comes from the combustion of the injected fuel. For a given set of initial conditions, the conditions present after the compression stroke in the diesel cycle, a specific fuel will burn at a specific temperature, known as the flame temperature (T_f), which is dependent on the chemical composition of the fuel and the associated chemical kinetics with the air in the chamber.

Because the entire diesel cycle is driven by the power stroke, the fuel combustion event and associated heat-release rate control the timing of the engine. Due to the momentum of the cam shaft, if the fuel does not combust at the proper moment the stroke may be shortened and less power available to the engine. The delay from the moment at which fuel is injected to the beginning of the combustion event is referred to as the ignition delay (ID). A particular fuel will have a particular ID that depends on the injection environment, temperature and pressure in the chamber at the time of injection. In order to maximize the power output of an engine, and thus increase its efficiency, fuel injection must be properly timed such that combustion begins at the proper moment and occurs at an acceptable rate during the cycle. Because of the cycle's dependence, the combustion event has been, and continues to be, researched.

In Compression-Ignition (CI) engines, the combustion event is commonly characterized by two measurements, the ignition delay (ID) and the heat-release rate (HRR). These two properties control the performance of the power stroke and the timing of the engine, and therefore generate the motivation for extensive research on both of these characteristics.

4. Ignition Delay

The ignition delay, ID, is defined as "the period between the start of fuel injection into the combustion chamber (SOI) and the start of combustion (SOC)" [18]. Heywood presents Equation (2) as the general correlation for ID, which he refers to as τ_{id}.

$$\tau_{id} = Ap^{-n} \exp\left(\frac{E_A}{\tilde{R}T}\right) \quad (2)$$

where A and n are constants dependent on the fuel, E_A is the apparent activation energy for the fuel, $\tilde{R}$ is the universal gas constant and T and p are the chamber temperature and pressure at SOI.

The ID for a CI engine is composed of two parts, the physical delay and the chemical delay. The physical delay relates to the time between the beginning of injection and the initial stages of the subsequent combustion process [19]. During the physical delay period the fuel is "atomized, vaporized, mixed with air, and raised in temperature" [19]. The chemical delay relates to the time required for the chemical reaction to occur. Because the injection is not homogeneous throughout the spray, the edges of the jet will be exposed to more oxidizing air than the inner regions and fuel droplets will be different sizes and in different stages of vaporization; therefore, combustion is not uniform throughout the reaction. The sum of the physical and chemical delays results in the overall ignition delay, the determination of which is the objective of this study.

5. Physical Delay

a. Fuel Injection

In order to maximize efficiency and performance of diesel engines, fuel injectors are designed to deliver a specific amount of fuel into the cylinder at a specific moment in the engine cycle. The typical operating conditions at the time of injection are shown in Table 2. In addition to meeting the engine cycling requirements, fuel injectors are also designed to take advantage of specific fuel properties in order to maximize the effect of the combustion. Before autoignition can occur, the liquid fuel must undergo a phase change from the liquid to a vapor state. Because diesel engines operate on a continuous cycle, this transformation must happen quickly in order to maximize the effect of the power stroke. In addition to minimizing the time required to complete the phase transformation, fuel injectors are also designed to spread the fuel uniformly throughout the entire chamber to result in a more uniform burn.

Table 2 Typical chamber conditions at fuel injection, from [18].

Property	Condition
Pressure	50 to 100 atm
Temperature	~1000 K
Density	15 - 25 kg/m3

Figure 6 shows a diagram of the spray structure for a typical fuel injector. The liquid jet leaves the nozzle, and becomes turbulent. As the distance from the injector tip increases, mixing and entrainment with the air in the chamber cause the fuel to spread out.

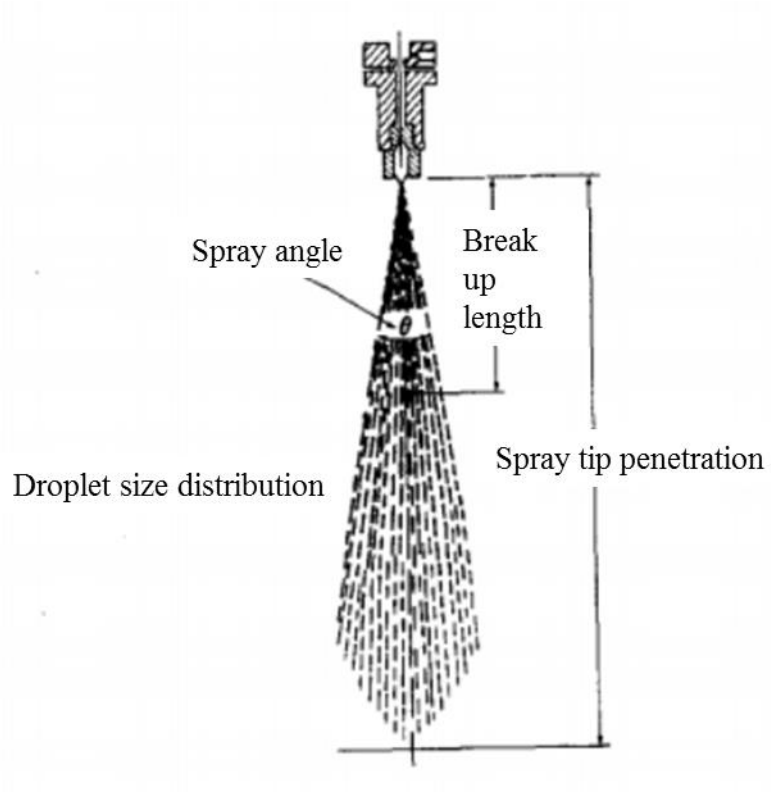

Figure 6 Characteristic fuel injection, from [18].

b. Atomization

Atomization is the process by which the liquid jet of fuel forms into smaller droplets. This phenomenon is dependent primarily on Reynolds number and Weber

number, and thus is driven by a combination of the physical design of the specific injector and the fluid properties of the fuel.

The Reynolds number (Re_d) is the ratio of inertial forces and viscous forces for a flow and is shown in Equation (3)

$$\mathrm{Re}_d = \frac{\rho u d}{\mu} \tag{3}$$

where ρ is the density of the fluid, u is the velocity of the fluid, d is the characteristic diameter, and μ is the dynamic viscosity of the fluid. As the ratio between the inertial and viscous forces increase, the droplet size decreases and the atomization rate increase. At low Reynolds numbers, the breakup process is driven by surface tension forces and results in droplet sizes larger than the jet diameter. As the injection velocity increases, viscous effects between the fuel and the surrounding air, as well as the surface tension forces result in a droplet size on the order of the jet diameter. At very high Reynolds number, the droplet breakout is driven by aerodynamic interactions between the fuel in the jet and the surrounding air. At these high Reynolds numbers, the droplet size is on the order of 10 μm [18]. It is important that injectors have high tip pressures and small jet diameters to be able to induce high Reynolds number flows. Typical injection velocities are on the order of 100 m/s [18].

Similar to the Reynolds number, the Weber number (We) is defined by Kuo [20] to be the ratio of the aerodynamic force and the surface tension force for a flow and is shown in Equation (4),

$$We = \frac{\rho \left| v_P - v_g \right|^2 d}{2\sigma_s} \tag{4}$$

where ρ is the density of the fluid, v_P is the velocity of the droplet, v_g is the velocity of the surrounding fluid, d is the characteristic diameter of the droplet, and σ_s is the surface tension force. As the ratio between the two forces increases, the break up process accelerates, and the rate of atomization increases.

Depending on the relationship between the Reynolds and Weber numbers, the atomization process may follow different breakup types. For $0.2 \le We\,\mathrm{Re}_d^{-0.5} \le 1.6$ the

droplet breakup process follows the "parachute type" model, where the flow causes the droplet to flatten and eventually break into a group of small droplets, along the line of the flow. For $1.0 \le We\,\mathrm{Re}_d^{-0.5} \le 20$ the breakup process follows the "stripping type" model, where the viscous forces from the flow tear shrouds off the flattened droplet. For $20 \le We\,\mathrm{Re}_d^{-0.5} \le 200$, the breakup process follows the "explosion type" model where the droplet instantly shatters into many smaller particles [20]. Because the droplet breakup process is continuous, the fuel spray being injected in CI engines typically undergoes all three of these types of droplet breakup processes.

c. Spray Penetration

The magnitude of the spray penetration is another important factor in the combustion event. Depending on the operating conditions of the engine, the size of the chamber, and the presence of air swirl design of the engine, the penetration depth for an injection may vary. In the design of a diesel engine, this depth is thoroughly researched and characterized. Equation (5) shows the empirical correlation that best predicts S, the spray penetration length:

$$S = 3.07\left(\frac{\Delta p}{\rho_g}\right)^{1/4}\left(td_n\right)^{1/2}\left(\frac{294}{T_g}\right)^{1/4} \qquad (5)$$

where Δp is the pressure drop across the injector nozzle, t is the time after the start of injection, d_n is the injector nozzle diameter, and T_g and ρ_g are the temperature and density of the mixture in the chamber [18]. It is clear from the equation that the spray penetration length is dependent on the physical properties of the injector, rather than the properties of the specific fuel being injected into the chamber. Based on this relationship, the ID for a specific fuel is expected to change for different injectors.

d. Droplet Evaporation

The atomization process results in a spray of very small, liquid droplets leaving the tip of the injector. In order for combustion to occur, these fuel droplets must mix with

the air. This mixing is accomplished through evaporation. Heywood [18] gives three steps in the process of droplet evaporation:

- Deceleration of the drop due to aerodynamic drag
- Heat transfer to the drop from the air
- Mass transfer of vaporized fuel away from the drop

The first step in the evaporation process is directly dependent on the atomization properties of the fuel. For a given engine, the viscous properties of air are not going to change; however, the drag forces on the individual droplets will vary with droplet size. Heat transfer from the air in the chamber to the fuel droplet is also controlled by the droplet size. For the high speed droplets in the spray, convection from the air to the individual droplets is the principle mode of heat transfer. A smaller average droplet size results in a greater total surface area of the aggregate droplets, and thus more heat transfer. As the temperature of the droplets increase, the vapor pressure of the fuel increases and accelerates the evaporation process.

6. Chemical Delay

The Cetane number (CN) for a given fuel is a measure of the fuel's tendency to autoignite and is used to qualify the ignition quality of a fuel [21]. The CN is directly dependent on a fuel's molecular composition. Straight-chain Paraffinic compounds have a high ignition quality, while aromatics and alcohols have a poor ignition quality [18]. Typical fuels are a combination of paraffinic, aromatic, and olefinic hydrocarbons. Figure 7 shows a plot of the CN – ID relationship for different fuels. The figure shows that fuels composed of a higher percentage of paraffinic chains tend to have a higher CN and a shorter ID. Conversely, the figure shows that fuels composed of a higher percentage of aromatics generally have a lower CN and a higher ID.

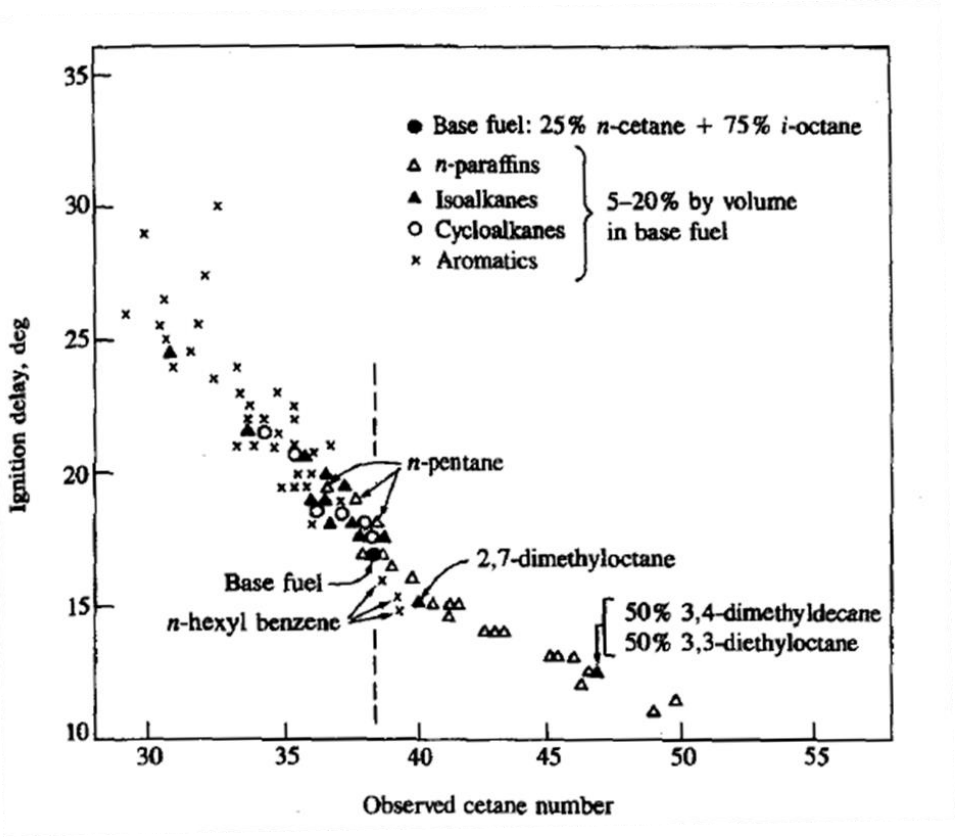

Figure 7 CN versus ID for varying fuels, from [18].

7. Heat-Release Rate

Heat-Release Rate (HRR) is defined as "the rate at which the chemical energy of the fuel is released by the combustion process" [18]. Similar to how the ID characterizes the physical and chemical processes occurring before start of combustion (SOC), the HRR characterizes the physical and chemical process occurring after SOC. Figure 8 shows a plot of a typical HRR for a CI engine. Following the ID, Heywood [18] divides the HRR into three phases, shown in Figure 8.

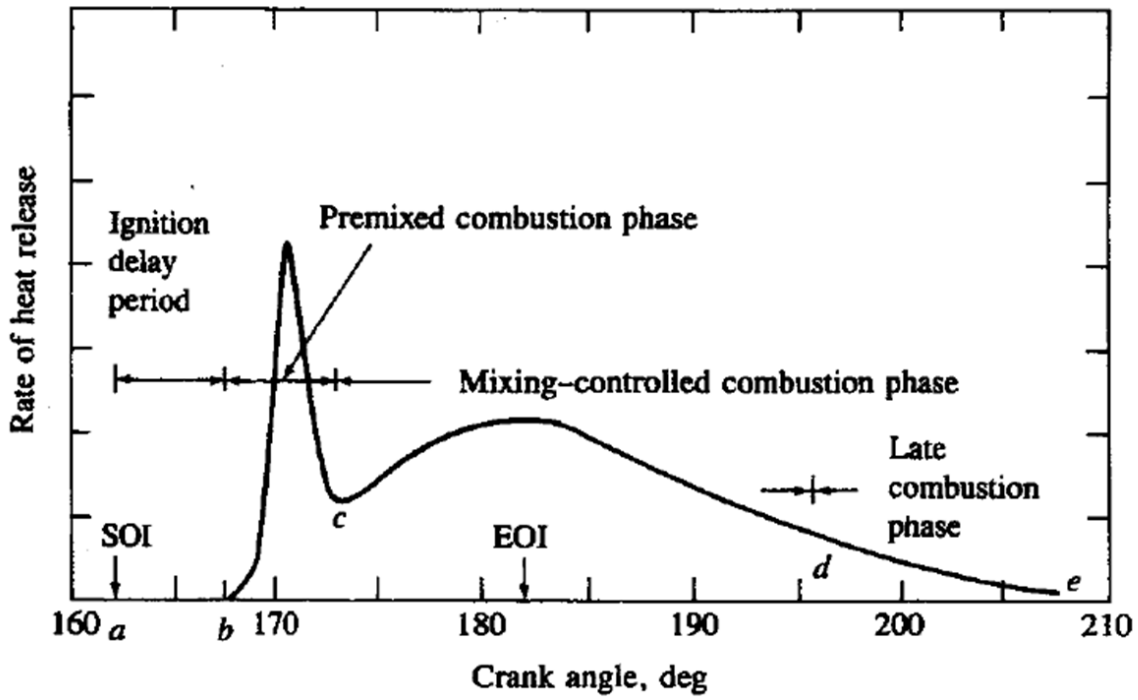

Figure 8 Typical HRR plot in diesel engines, from [18].

The "premixed" phase begins directly after SOC. Rapid combustion occurs in this phase due to the fuel/air mixing that occurred during the ID phase. The HRR peaks during this phase. The HRR during the "mixing-controlled" phase are limited by the mixing rate between the remaining fuel and air. The same processes that occurred leading up to the SOC, atomization, droplet evaporation, and air-fuel mixing, are present during this stage, as well as the chemical kinetics driving the combustion reaction. However, due to the higher temperatures and pressures that resulted from the premixed stage, the air-fuel vapor mixing rate is the limiting factor. As discussed previously, only the outer edges of the fuel are exposed to air, and thus allow mixing to occur. Once the outer edge of the fuel ignites, time is required for the air to mix with the newly available vaporized fuel. The final stage in the combustion event is the "late combustion" phase. In this phase, any excess fuel is burned. Although the exact amount of fuel injected to the chamber is controlled by the injector, nonuniform conditions in the chamber result in either unburned fuel or fuel-rich combustion products, which combust during this phase.

Peterson conducted a study to compare the HRR of HRD fuel and conventional, F-76 diesel fuel using a two-stroke, direct injected Detroit 3-53 Diesel engine [22]. Figure 9 shows the results from the study. Although the peak of the HRR for the engine was lower using the HRD fuel, the engine was able to successfully operate. It is important to note that this figure shows the results for "neat" HRD, meaning a 100% HRD fuel. The plot also shows that the premixed combustion stage for the HRD fuel was shorter than that for F-76; however, this did not have a negative impact on the performance of the engine. Peterson's study concluded that the combustion performance of the HRD fuel was comparable to F-76. Based on the HRR results, Peterson confirms that HRD would be an effective drop-in fuel replacement for F-76, for his specific engine. Due to the nature of his research, taking data from an actual engine, Peterson was unable to conclusively determine SOI during testing. Without determining SOI, the ID could not be characterized. This thesis builds on Peterson's results, and focuses on determining the ID for HRD fuels, on various Navy-relevant diesel injectors.

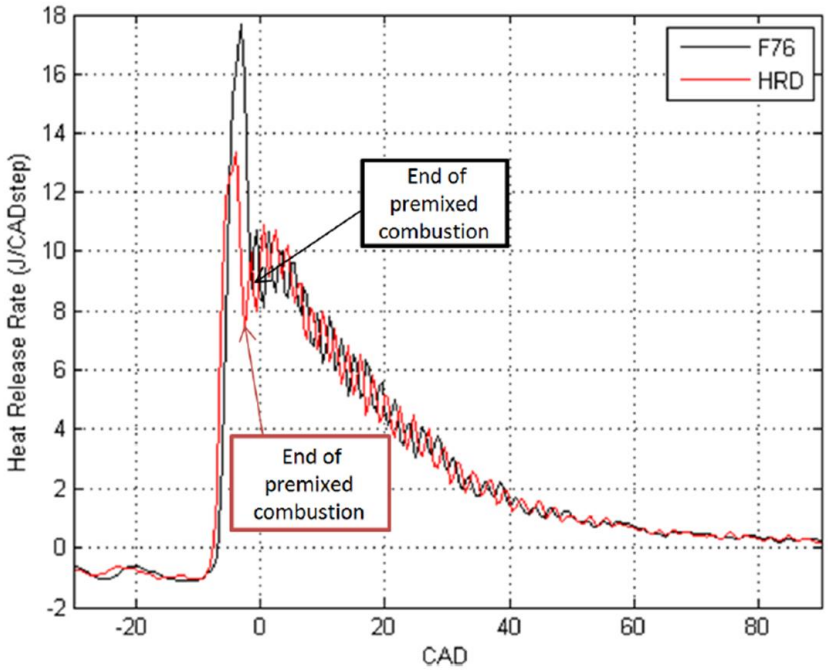

Figure 9 HRR, HRD and F-76 at 1,650 rpm 150 ft-lbs, from [22].

II. THE TESTING APPARATUS

A. THE TESTING OBJECTIVES

1. Objective

The objective of this experiment was to determine the injector-specific ignition characteristics of an F-76-HRD 50/50 blend fuel and an F-76-DSH 50/50 blend fuel. First, the testing apparatus was evaluated using the Sturman injector and conventional F-76 diesel fuel. The ignition delay values for this case were compared with previously published results to show that the testing apparatus was capable of reproducing the previously published ignition delay times. Second, the ignition delay time at varying temperatures for each of the test fuels was determined using the Yanmar injector. Finally, the ignition delay at varying temperatures was determined for the same fuels but using the EMD injector. For each test case, the ignition characteristics for the alternative fuels were compared with the ignition characteristics found for the F-76 fuel using the same testing conditions. The overall results for this experiment are ignition delay vs. temperature relationships for each of the different fuels and injectors.

2. Measurements

In order to fulfill the testing goals, three measurements needed to be determined: the temperature at start of injection (SOI), the time at SOI, and the time at start of combustion (SOC). The ignition delay time for each injection temperature could then be calculated as the difference between the start of injection and the start of combustion. The testing apparatus for this research needed to be able to accurately and consistently capture these three measurements for each test run.

3. Testing Apparatus

The testing apparatus used for this research was developed by Warren Fischer during the course of his thesis [8]. A picture of the entire system is shown in Figure 10. The system is capable of simulating the TDC position of the piston in a diesel engine. A high strength pressure vessel contains the combustion event. The high temperature and

pressure is generated using an ethylene-air preburn. When the desired conditions are reached, a fuel injector sprays the fuel into the chamber for the ignition event. The ignition characteristics of different fuels in different Navy-relevant fuel injectors were investigated in this experiment and determined through data obtained via optical imaging, fine gage thermocouple measurements, and dynamic pressure measurements.

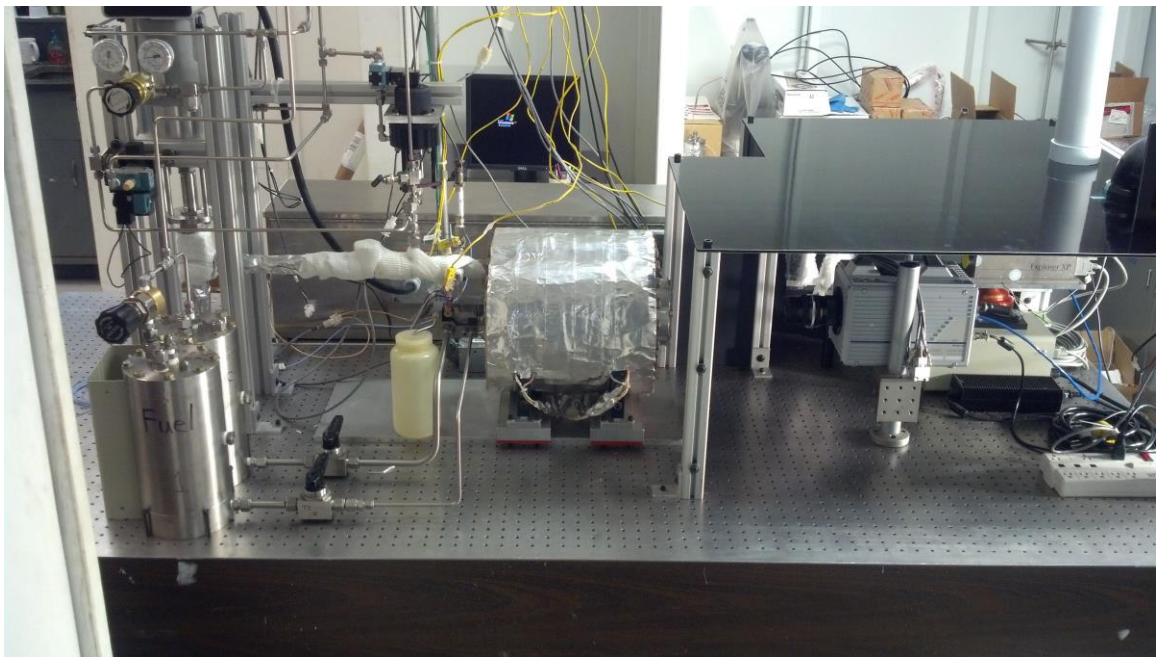

Figure 10 Rocket lab testing apparatus

B. THE COMBUSTION BOMB

1. Constant Volume Combustion Chamber

The Constant Volume Combustion Chamber (CVCC) was used to simulate the operating conditions of the Top-Dead-Center (TDC) piston position preceding the power stroke in a diesel engine. In order to properly simulate these conditions, the pressure chamber must be capable of withstanding high temperatures and high pressures and possess specific measurement capabilities: thermocouple ports, pressure ports, and optical imaging access. Figure 11 shows the combustion chamber assembly used for this research. Small modifications to improve access to the chamber were added to the work done by Fischer [8]. As shown in the figure, the chamber has a modular design which

allows the chamber to be utilized for testing injectors of different sizes. The chamber was constructed of a heat-treated, 17-4 stainless steel that is capable of operating at design pressures up to 3,000 psi. The chamber is capable of operating at nominal bulk temperatures up to 500 degrees Fahrenheit. At these maximum temperatures, Fischer [8] determined that the assembled chamber has a minimum factor of safety of 6.1. When assembled, the chamber is cylindrical and has an inside diameter of 8.2 in. and a length of 8.0 in. One end of the chamber is the optical flange, which houses a sapphire optical window, through which imaging devices have access to the combustion reaction.

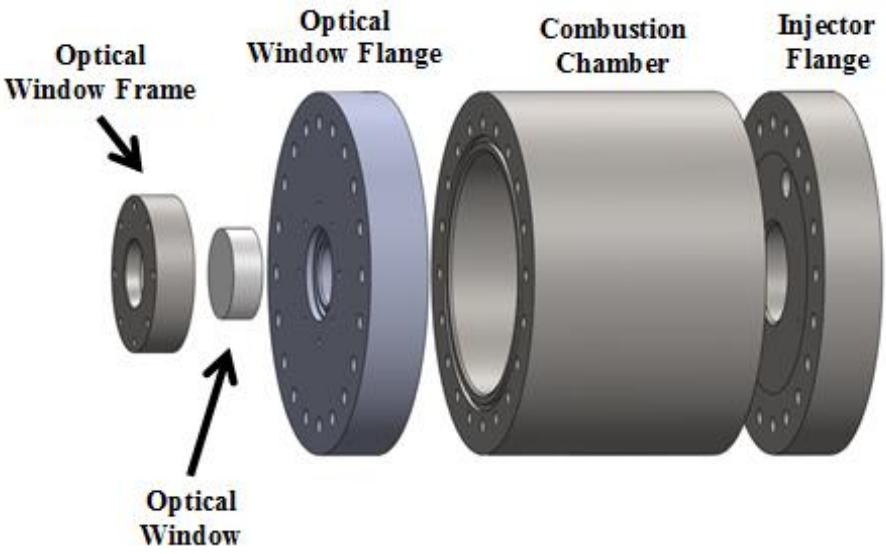

Figure 11 Combustion chamber exploded view, after [8].

The opposite end of the chamber connects to the injector flange, shown individually in Figure 12. This flange contains a large port capable of fitting each of the test injectors selected for testing. The injector flange also has a 1-1/16 inch port through which high pressure gases can be either supplied or exhausted. The three smaller, 7/16 inch ports at the 3, 6, and 9 o'clock positions around the injector port were added to the original work developed by Fischer [8]. The engineering drawing for the flange modifications is shown in Appendix A. These ports give access to the inside of the chamber for either temperature or pressure transducers, and significantly increased the quality of data obtained in testing.

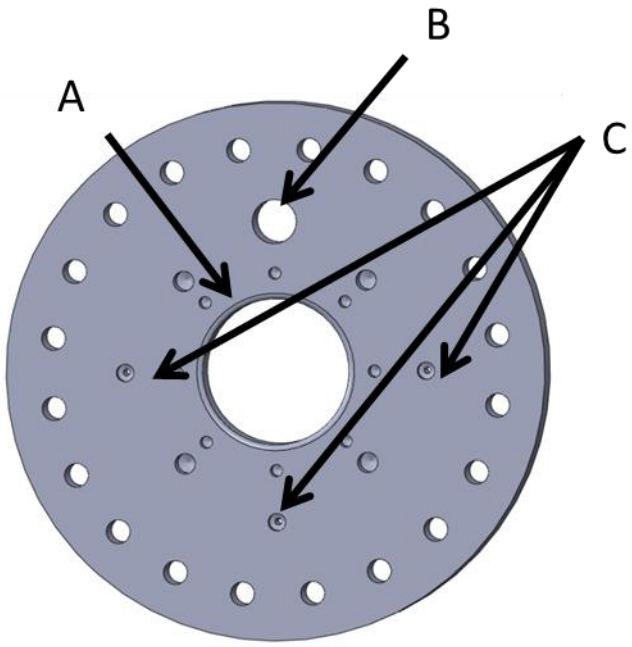

Figure 12 Injector flange, A) injector orifice, B) high pressure gas addition and exhaustion port, C) through ports for temperature and pressure transducers, after [8].

As outlined in the work done by Fischer [8], all pressure seals were achieved using O-rings. Both the optical and injector flanges and the optical window frame each had O-ring grooves machined in at the proper radius. Viton O-rings, capable of withstanding high temperatures, were used to seal each orifice. No signs of leakage were observed or measured during the testing process.

2. Preburn

In order to properly simulate TDC, the preburn needed to increase the temperature and pressure inside the chamber to result in a uniform mixture of high temperature air.

a. Chamber Temperature Requirements

Depending on their location and operating conditions, diesel engines produce post-compression temperatures ranging from 700 K to 1,300 K. The preburn needed to be hot enough to raise the temperature of the entire chamber to this range. Additionally, the

preburn needed to be repeatable to the point that fuel injections could be repeatedly conducted at specific temperatures across the aforementioned range.

b. Chamber Pressure Requirements

Typical diesel engines operate at standard temperature and pressure (STP) with a volumetric compression ratio ranging from 14:1 to 20:1. The actual compression ratio changes based on the temperature and pressure conditions where the engine is operating. Based on the material limitations of the combustion chamber, volumetric compression ratios of 6.35:1 and 12.3:1 were chosen for this study. These settings resulted in chamber densities of 7.65 kg/m^3 14.8 kg/m^3 respectively, capturing the lowest end of actual, operating engine compression ratios. Ideally, the product of the preburn reaction would be air at high pressure and temperature, conditions reflective of TDC conditions. In order to achieve this state, it was necessary to control the products from the preburn reaction. Because data collection relied on high-speed imaging, it was essential that soot and other particulates be limited in the products. Also important was controlling the amount of water in the reactants, both for its effect on the combustion kinetics and its tendency to obscure optical images by condensing on the optical window. Condensation from the preburn was prevented by heating the walls of the chamber to a nominal temperature of 420 K.

c. Preburn Mixture

Hydrogen-oxygen preburns have typically been the main choice in combustion bomb testing. The mixture reacts easily, and yields the required high pressures and temperatures. It also burns completely clean, meaning that no soot particles would be formed that could potentially obscure the high quality imaging. Along with these benefits, the hydrogen-oxygen preburn also has two main disadvantages: 1) stratification of the hydrogen gas results in a stratified mixture, and 2) the hydrogen-oxygen reaction produces significant amounts of H_2O. Of these two disadvantages, the stratification of the mixture is the more significant. Because hydrogen is so much lighter than air, the preburn reaction tends to occur at different conditions at the top of the chamber, and the increase in temperature and pressure is not seen uniformly throughout the chamber. This unequal

distribution of temperature would result in inconsistent injection temperatures for the actual ignition testing experiments. The effect of the stratification is so great, that Picket et al. [23] added a mixing fan inside the chamber to more uniformly distribute the preburn mixture. This fan added additional constraints to the experiment, such as added complexity, servicing/replacing the fan, approximating the distribution of the preburn mixture.

Another type of preburn utilizes an ethylene-air mixture. As with the hydrogen-oxygen case, the hydrocarbon preburn is able to yield the required temperatures and pressures. The greatest advantage of the ethylene preburn is the inherently uniform distribution throughout the chamber. Ethylene and air have similar molecular weights, and thus the temperature and pressure of the chamber are increased uniformly throughout, without the need of any additional equipment such as a mixing fan. Different from hydrogen, the ethylene preburn does not produce large quantities of H_2O, which decreases the amount available for condensation onto the optic window. Unfortunately, the reaction does not always burn clean, and soot as well as unburned carbon are possible products of the reaction, especially at higher temperature conditions. For this study, the ethylene-air preburn was used. The uniformity of the reaction products outweighed the presence of solid particulate products which appeared to be minimal. Because the ethylene preburn required the oxygen in air to react with the ethylene for the preburn reaction, makeup oxygen was included into the preburn mixture in order to result in a post-preburn chamber environment containing approximately 20% oxygen, similar proportions as the air found at TDC in diesel engines.

d. Preburn Implementation

The preburn was implemented in stages. First, the combustion chamber was evacuated. It was assumed that the only remaining substance in the chamber, if any, was pure air. The combustion chamber was then filled with a lean mixture of the ethylene-air reactants, using partial pressures. At this point, the makeup oxygen was also filled into the chamber. In another, smaller chamber, a high-pressure ethylene-air “fuel plug” was created using a stoichiometric mixture ratio, approximately 6.78% ethylene. The preburn

event consisted of opening the line connecting the high pressure, stoichiometric mixture with the chamber. At the same time, a spark plug was ignited using a Plasma Pulse Generator. The stoichiometric mixture ignited and then traveled to the combustion chamber and ignited the lean mixture.

In order to reach different temperatures for SOI, different amounts of ethylene were used in the lean mixture. Figure 13 shows a temperature plot versus time of the preburn event in the chamber for a 3% ethylene mixture at an initial chamber operating pressure of approximately 100 psi.

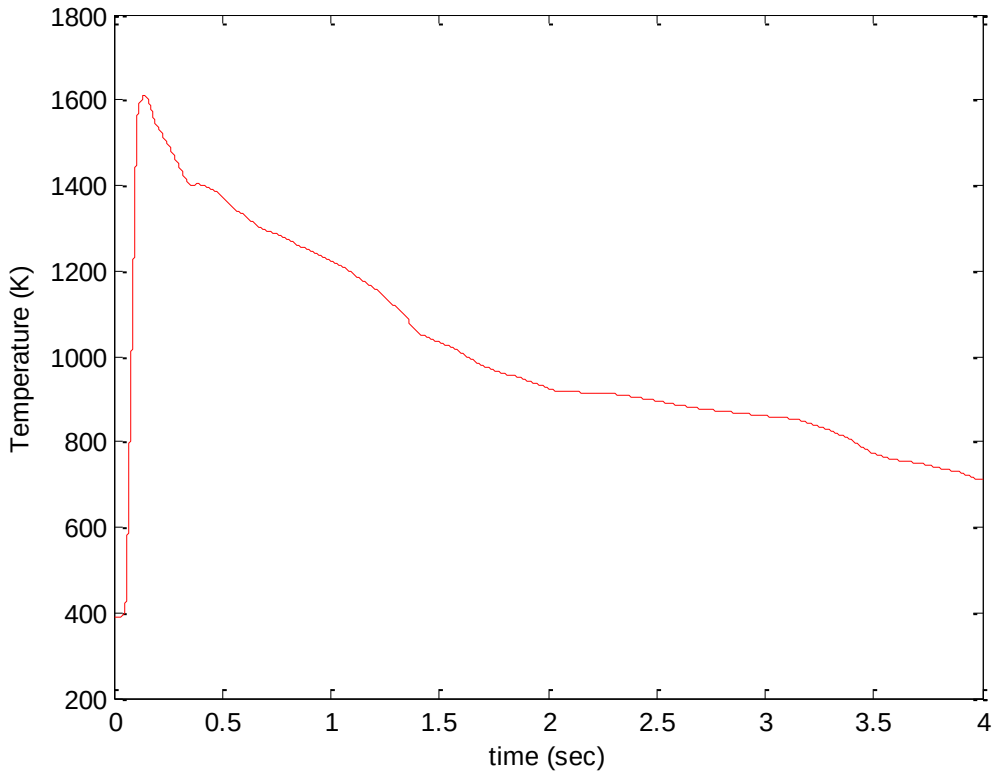

Figure 13 Typical preburn temperature plot

The plot shows that the temperature peaks very quickly, and then slowly trails off. The leading edge of the temperature curve is changing rapidly, while the trailing edge of the temperature curve is smooth and continuous; because of this relationship, it was desirable that the fuel be injected on the trailing edge of the preburn. For example, a

delay of 0.8 seconds corresponds to an injection temperature of approximately 1200 K while a delay of 1.4 seconds corresponds to a temperature of approximately 1000 K. The temperature plot for a preburn mixture of 2% ethylene follows the same trend as the 3% case, but the peak temperature is significantly lower. With the more lean mixture, lower injection temperatures could be reached.

The functioning of the chamber depended on heat from the preburn being dissipated through the relatively cold chamber walls, resulting in the curve shown in Figure 13. Because water was a product of the preburn reaction, water could condense on the cold walls and especially the even cooler optical window. This interfered with the quality of the images captured. This negative effect of the preburn was overcome by the installation of a heating wrap that heated the walls of the chamber. When the ambient temperature of the walls reached approximately 260 °F, the water no longer condensed on the optical window and was no longer an issue.

3. Fuel Injection

Once the preburn brought the combustion chamber to the desired operating conditions, the test fuel was injected into the chamber. As discussed, the injection temperature was controlled by delaying the SOI event. This delay was directly programmed in to the BNC signal generator that received the trigger from the LabView code. Throughout the testing, the delay ranged from 0.8 seconds to 1.5 seconds. The BNC signal generator then passed the SOI signal to the injector controller. As mentioned in the introduction, three different injectors were tested throughout the research. Because each of the injectors actuate differently, each required different modifications to the timing and testing apparatus. These modifications are discussed in this section.

*a. **Sturman Injector***

The BNC signal was sent to a high-powered driver that activated a fast-acting spool valve. This valve delivered 3,000 psi hydraulic fluid to the Sturman injector. At the tip of the injector, the hydraulic fluid compressed the test fuel to a 6:1 pressure ratio. The fuel sprayed out of the injector at approximately 18,000 psi. Figure 14 shows an image of the Sturman spray. The fuel leaves the injector in a continuous ring. Because of the high

tip pressure, the fuel vaporizes quickly as it leaves the injector. The small, black circle in the image is the injector tip and the light is the fuel expanding radially from the injector tip.

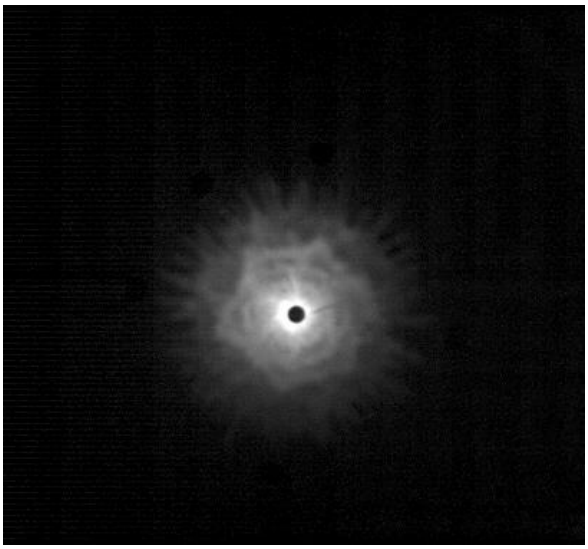

Figure 14 Sturman injection image

b. Yanmar Injector

The Yanmar injector actuation differed significantly from the Sturman. Rather than using hydraulic fluid to compress fuel at the tip of the injector, the Yanmar required high pressure fuel, over 3,500 psi, to "crack" the nozzle tip plunger. The BNC signal was relayed to a 24 VDC relay that controlled a high-pressure, Clark-Cooper solenoid valve. This valve was connected to a nitrogen tank with a regulated pressure of 4,500 psi. The set up for the Yanmar injector is shown in Figure 15 and Figure 16.

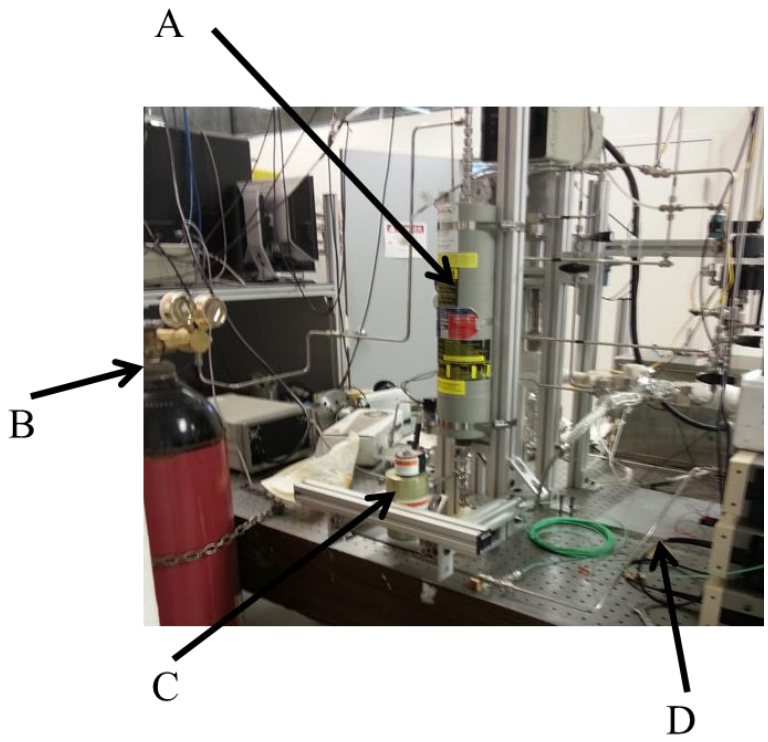

Figure 15 Yanmar injector setup: A) high pressure accumulator, B) high pressure nitrogen, C) high pressure Clark-Cooper valve, D) high pressure fuel line

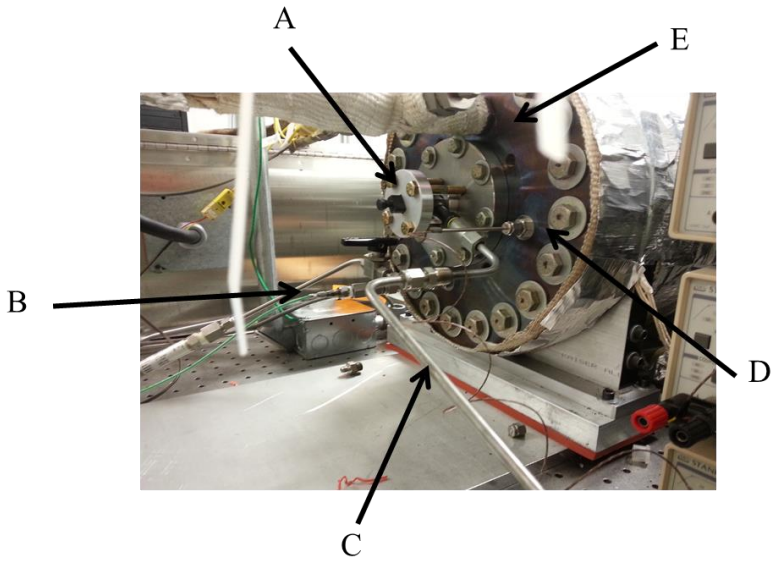

Figure 16 Yanmar injector setup: A) Yanmar fuel injector, B) pressure transducers, C) high pressure fuel line, D) thermocouple transducer, E) combustion chamber

Once cracked, the fuel sprayed through the nozzle until the pressure dipped below 3,500 psi. A pulse width of 0.1 seconds was used for the BNC signal to control the Yanmar injector. Figure 17 shows an image of the Yanmar spray and subsequent ignition. It is characterized by the six jets arranged concentrically about the tip of the injector.

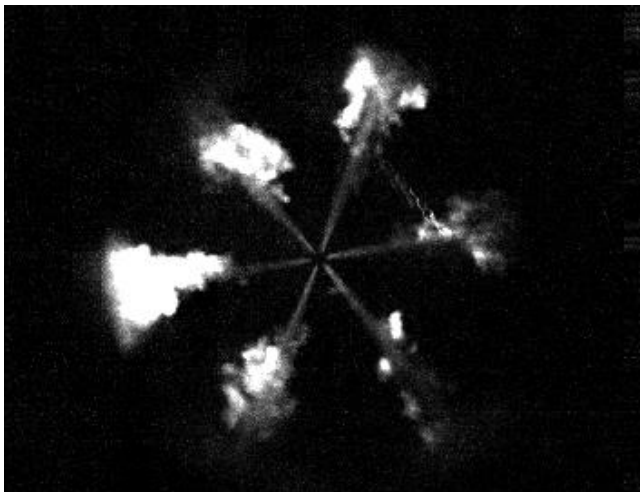

Figure 17 Yanmar injection/ignition image

c. EMD Injector

Ideally, the EMD testing setup would be capable of producing a stroke similar to the cam stroke of an engine operating at 900 rpm, which results in an injector plunger velocity of 78 in/sec. The Miller HV3 hydraulic piston was used to deliver the ramming force on the fuel injector. This piston has a bore diameter of 2 in., a stroke length of 2 in., and a maximum operating pressure of 2500 psi. The piston and injector were coupled to the injector flange of the combustion chamber using 4, 1/2” – 20 grade 8 all-thread bolts, sheathed by 3/4" thick-walled steel tubing. This coupling is shown in Figure 18.

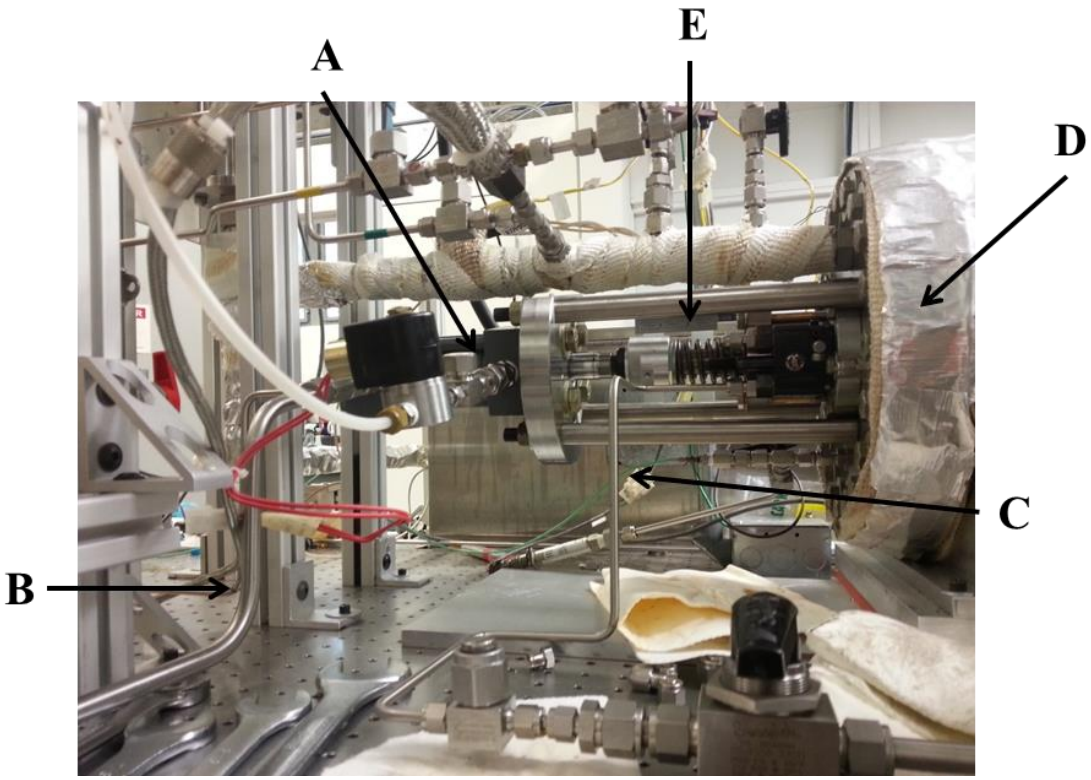

Figure 18 Hydraulic piston/EMD injector coupling: A) hydraulic piston, B) piston hydraulic oil input line, C) injector fuel input line, D) combustion chamber, E) EMD injector

The hydraulic fluid used to actuate the piston was stored in the same high pressure accumulator, used for the Yanmar injector. The Clark-Cooper high pressure valve requires a minimum pressure differential of 100 psi in order to maintaining the "closed" position. [24, p. 50] It was discovered that applying 100 psi to the hydraulic piston was enough to compress the spring and actuate the EMD injector, albeit at a very slow rate, and the Clark-Cooper valve could not be used for the EMD testing. The valve worked satisfactorily for the Yanmar injector which had a cracking pressure of approx. 3500 psi. Initially, the Clark-Cooper valve was replaced with an electronically actuated, shop air driven 1/4" Swagelok quarter-turn ball valve. 1/4" tubing was used to connect the valve to the piston. Initial tests shown in Table 3, show that at the maximum operating conditions for the hydraulic piston, the injector plunger velocity maxed out at 17.06 in/sec using the 1/4" valve and tubing. In an attempt to increase the plunger velocity, both the 1/4" valve and tubing was replaced with 1/2" components. As shown in Table 3, the

injector plunger velocity for this configuration reached its maximum at 33.7 in/sec, nearly twice that of the 1/4” configuration.

Table 3 Injector plunger velocity

Pressure (psi)	Plunger Velocity (in/s)	
	1/4" plumbing	1/2" plumbing
1000	7.68	21.32
1500	10.7	24.8
2000	14.09	31.24
2500	17.06	33.7

Although the maximum velocity of the plunger was less than half of the desired amount, the 1/2” configuration was used for testing in this project due to time and material constraints. This configuration is shown in Figure 19. For testing, the hydraulic fluid was stored at 2500 psi in the high pressure accumulator. Fuel was supplied to the injector at 60 psi.

Figure 19 EMD injector setup: A) hydraulic piston, B) high pressure accumulator, C) spent hydraulic fluid, D) 1/2" ball valve, E) EMD injector, F) injector fuel tank

Figure 20 shows an image of the fuel just after the start of injection. Similar to the Yanmar injector, the fuel sprayed from the nozzle in a circular pattern with 6 different injection ports and subsequent ignition can be observed.

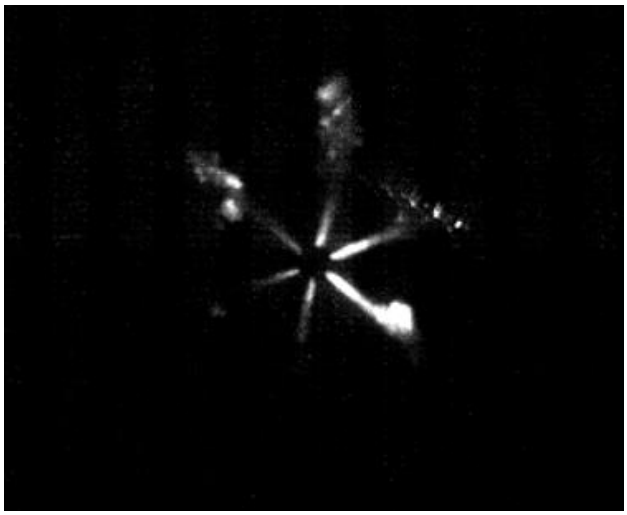

Figure 20 EMD injection/ignition image.

More work could be done to increase the speed of the plunger, and get closer to the 78 in/sec operating conditions. The outlet of the high pressure accumulator has a minimum diameter of 3/8", and limits the flow of hydraulic fluid at that point. This could be circumvented by either using a different accumulator, one with a larger minimum desire, or adding another accumulator to the line and thus supplying more fluid. These methods were not physically explored in the scope of this experiment.

4. Fuel Preparation and Delivery

For each of the different injectors, the fuel was prepared in the same manner by adding a pyrromethene 567A dye at trace amounts. Nominally less than 1 g/L were used and the dye had no effect on the properties of the individual fuel. Once dyed, the fuel was filtered and then placed into a specific storage chamber, depending on which injector was installed in the apparatus. Each fuel was tested in exactly the same way, and other than emptying to fuel storage chamber and purging the fuel lines, no additional modifications were needed to convert the testing apparatus from one fuel to another.

C. DATA COLLECTION

As mentioned previously, the temperature at SOI, the time at SOI, and the time at start of combustion are necessary in order to determine the ignition delay. This section focuses on outlining the methods used to capture this data.

1. Temperature at Start of Injection

The original design of the combustion chamber developed by Fischer [8] was modified in order to improve the resolution used to determine SOI. As shown in Figure 12, the modified flange has additional through ports at 90°, 180°, and 270° that allow better spatial resolution for the various transducers.

a. Pressure Sensors

The Injector Flange through port in the 180° position was tapped with both static and dynamic pressure gages, shown in Figure 21. The static pressure gage used was the Omega PX613-3KG5, with an operating range of 3000 psi and an absolute accuracy of 1%. Through calibration this uncertainty was reduced to 10 psi. Due to the high temperatures present in the combustion event, the static pressure gage was protected by distancing the physical location of the gage from the combustion event and filling the line with vacuum oil to prevent hot combustion production from damaging the gauge. As shown in Figure 21, the static pressure gage was removed approximately 1 foot from the combustion chamber. The hand valve was used to prevent the vacuum oil from being pulled out of the tube while vacuuming the combustion chamber. The dynamic pressure gage used for this experiment was a Kistler 603B1 high frequency quartz pressure sensor, which was calibrated to either 50 mU/V or 100 mU/V depending on the test case. This transducer is also shown in Figure 21. Due to a thin protective silicone coating, the high temperatures had no effect on the Kistler gauge. The actual pressure in the chamber at a given time is the sum of the static and dynamic pressures in the chamber at that time. Although the Kistler gages are capable of taking data at 50 Khz, data collection was limited to 10 Khz by the static pressure gage. The temperature in the chamber, with respect to time, was determined using the ideal gas law and the preburn density of 7.65 kg/m^3.

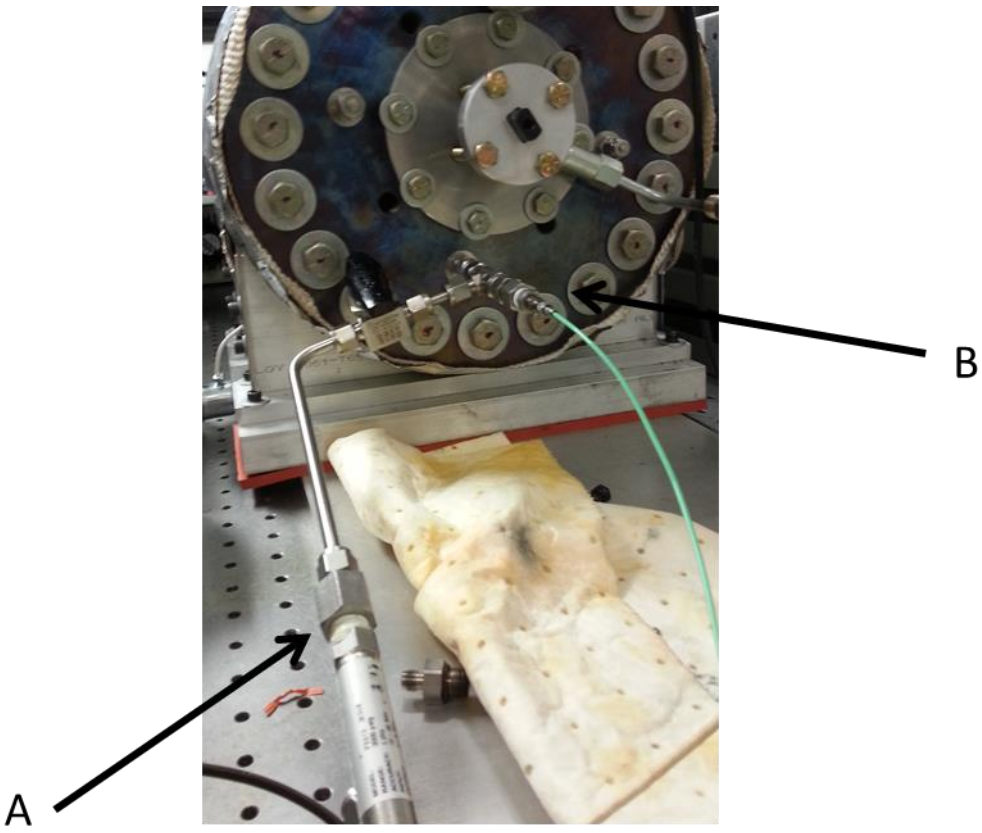

Figure 21 Pressure gauges , A) static pressure gauge B) Kistler dynamic pressure gauge

b. Thermocouples

The 90° and 270° positions on the injector flange allowed access into the chamber for the thermocouples. This allowed the thermocouples to be placed at various depths inside the chamber and provide temperatures for the actual combustion event. Because the combustion event occurs very quickly, the thermocouples needed to respond quickly to changes in temperature. Also, due to the nature of the combustion event, the thermocouples needed to be robust enough to withstand high temperatures. Unfortunately, the response time for a thermocouple typically decreases as its robustness increases. Large thermocouple junctions would have no trouble withstanding the high temperatures, but they were not sensitive enough to accurately measure the temperature. This challenge was overcome by specially preparing the thermocouples.

The Omega 5TC-GG-k-36-36, a 0.005 in. insulated thermocouple was the most effective thermocouple throughout testing. This thermocouple came insulated with a glass braid directly from the manufacturer which was rated up to 900 °F. The thermocouple was threaded through a 1/8 in. steel tube and sealed with epoxy on the trailing end. The steel tube was swaged to a 1/4 in. adapter on the outer face of the Injector Flange. The prepared 0.005 in. thermocouple is shown in Figure 22. After being prepared, the thermocouple was typically only capable of withstanding one combustion event.

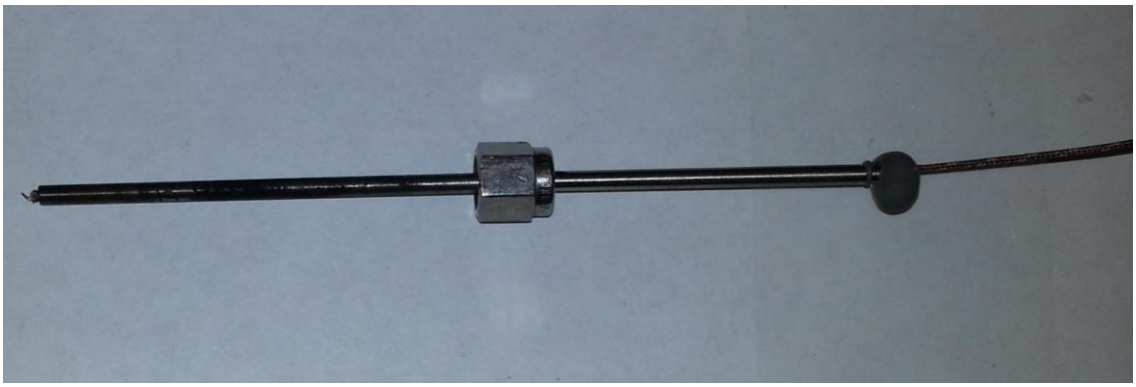

Figure 22 Prepared 0.005 in. thermocouple

The Omega 5TC-TT-k-40-36, a 0.003 in. also came insulated from the manufacturer and was used in the research. Initially, the 0.003 in. thermocouple was prepared the same as the 0.005 in. version; however, the perfluoroalkoxy (PFA) insulation was not as effective as the glass braid. On the testing apparatus validation runs consisting of solely the preburn, the 0.003 in. thermocouple was able to withstand approximately 3 runs before failing. When the heating wrap was applied with the chamber wall being heated to temperatures over 250 °F, the thermocouple was unable to withstand a single preburn event. In order to gather data using the 0.003 in. thermocouple, further changes were made to the preparation process.

Because the PFA coating was not rated for as high temperatures, the 0.003 in. thermocouple was additionally sheathed in a 1/8 in. ceramic tube, and then inserted into the 1/4 in. steel tube. The final product using this method is shown in Figure 23. The

addition of the ceramic sheath resulted in an additional epoxy seal. It was critical that the seal between the ceramic sheath and the steel tube not fail, thus creating a projectile out of the sheath and releasing the high pressure combustion gasses out of the chamber. In order to accomplish this, the epoxy was pulled into first the 1/8 in. ceramic sheathe, and then the 1/4 in. steel tube using a vacuum chamber. These additional preparations improved the life of the thermocouple to withstand one complete combustion event. When prepared in this method, the thermocouples never lost a pressure seal in the chamber.

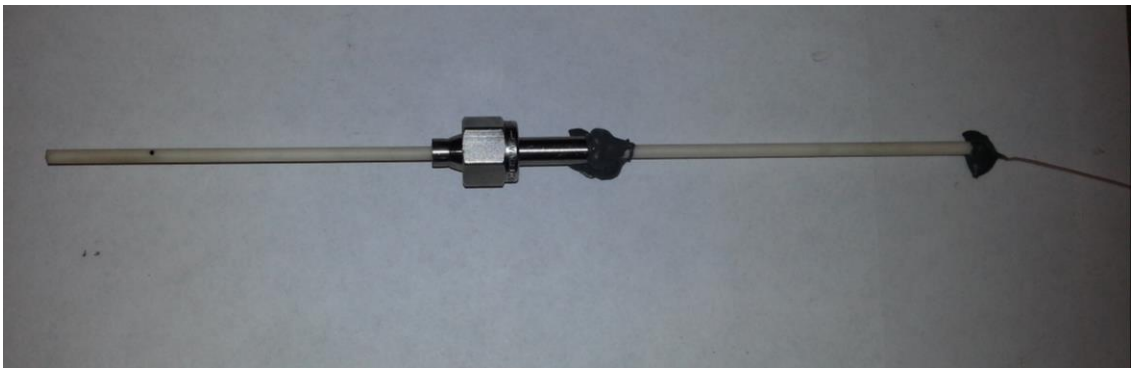

Figure 23 Prepared 0.003 in. thermocouple

After all the special preparations, both thermocouples were only able to withstand one complete combustion event due to the eventual failure of the junction/insulation late in the combustion event. This severely limited the temperature measuring capability throughout the testing. Using each desired preburn mixture, five tests were recorded and averaged together to create an average temperature plot for the given conditions. These plots are included in the results chapter. The SOI temperature from a given run was taken from corresponding preburn plot, based on the recorded time of injection. The error for this SOI temperature was taken as the standard deviation for the averaged preburns, and is shown in the final results as the horizontal error bars.

In an attempt to improve the accuracy of the results, new thermocouples were inserted on each run for certain test cases; however, the range of the SOI temperatures varied similar to the deviations seen from the average preburn plots. The average preburn

temperature plot was used as the primary means of determining the SOI because it had similar accuracy and was much more pragmatic.

2. Measuring the Ignition Delay (ID)

In order to determine the time difference between SOI and start of combustion, a high-speed imaging system was utilized, shown in Figure 24. The system is composed of a Photron FASTCAM SA5 high speed camera that was focused on the tip of the injector through the optical window. This camera is shown in Figure 25. The camera was set to capture images at 50 kHz with a resolution of 528 x 212 pixels. In order to reach this frame rate, the Explorer XP 532 nm laser was used to excite trace amounts of 567 nm emitting dye (Pyrromethene 567A) added to the fuel. The beam was focused to illuminate a 3 cm diameter area on the tip of the fuel injector. The laser was operated at 100% power and pulsed with a frequency of 100 kHz. A 570 nm narrow bandpass filter with a Full Width at Half Maximum (FWHM) of 10 nm was used on the camera to image the fluorescent fuel and protect the camera from the high-power laser emissions. A 4-bit shift was used in the image recording software in order to more easily process the images.

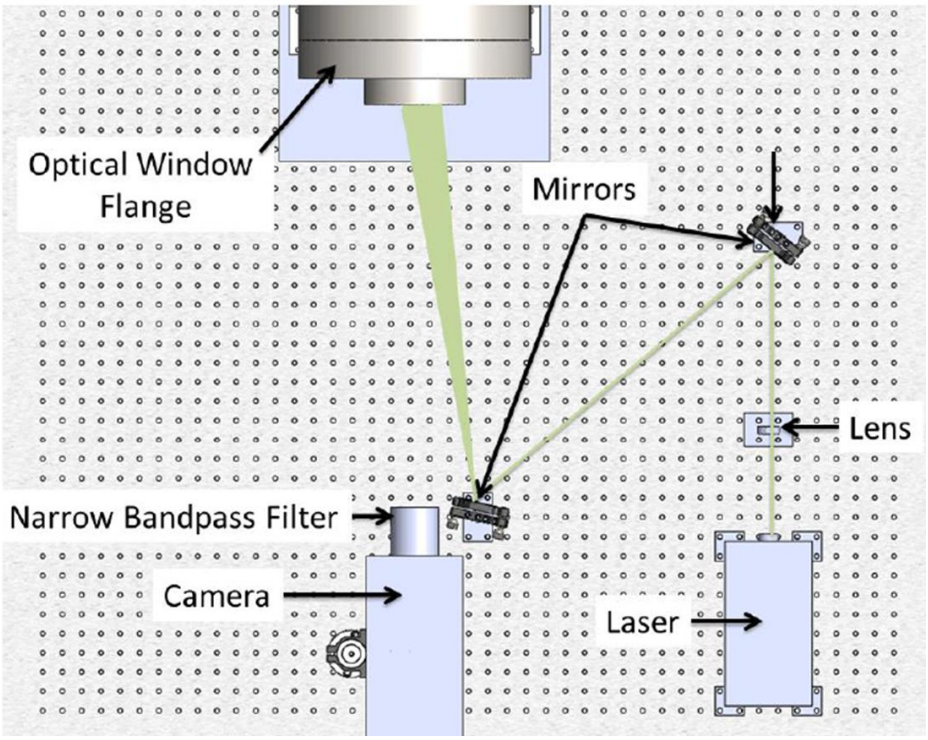

Figure 24 High speed imaging system, from [8].

Figure 25 Photron FASTCAM SA5, ultra high video system, from[25].

III. RESULTS AND DISCUSSION

A. DATA ANALYSIS

a. Start of Injection

Start of injection was defined to be the time that fuel initially appeared on the tip of the injector. Figure 26 shows the sequence of frames before and after SOI for the Yanmar injector. Visual inspection of the figure yields that injection occurred in either frame #112 or #113.

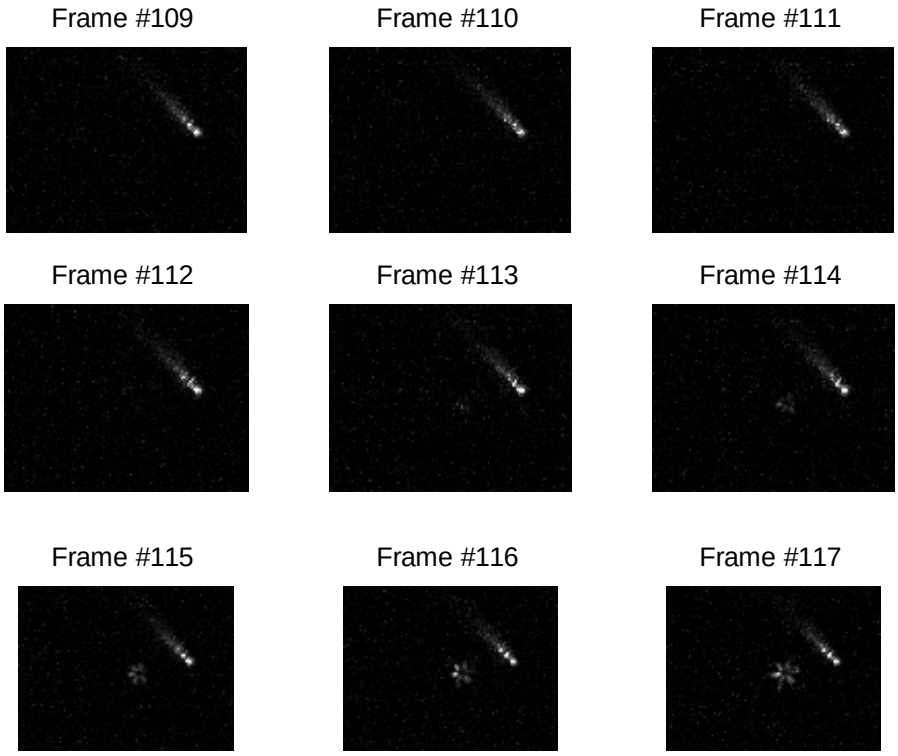

Figure 26 SOI image sequence

Rather than relying on visual observation of each individual combustion run to determine SOI, an image-processing code was used to automate the process. This code is included in Appendix B. Essentially, the code created a small box on the tip of the injector and used pixel averaging to determine the frame in which injection began. Figure

27 plots a typical pixel averaging sequence for a run using the Yanmar injector. It is clear that injection occurred when the slope of the plot began to increase. According to the code, SOI occurred in frame 112 for this particular run. This corresponds well with the visibly image determination shown in Figure 26. Each frame captured by the camera received a time stamp, and the time at SOI was determined from this time stamp.

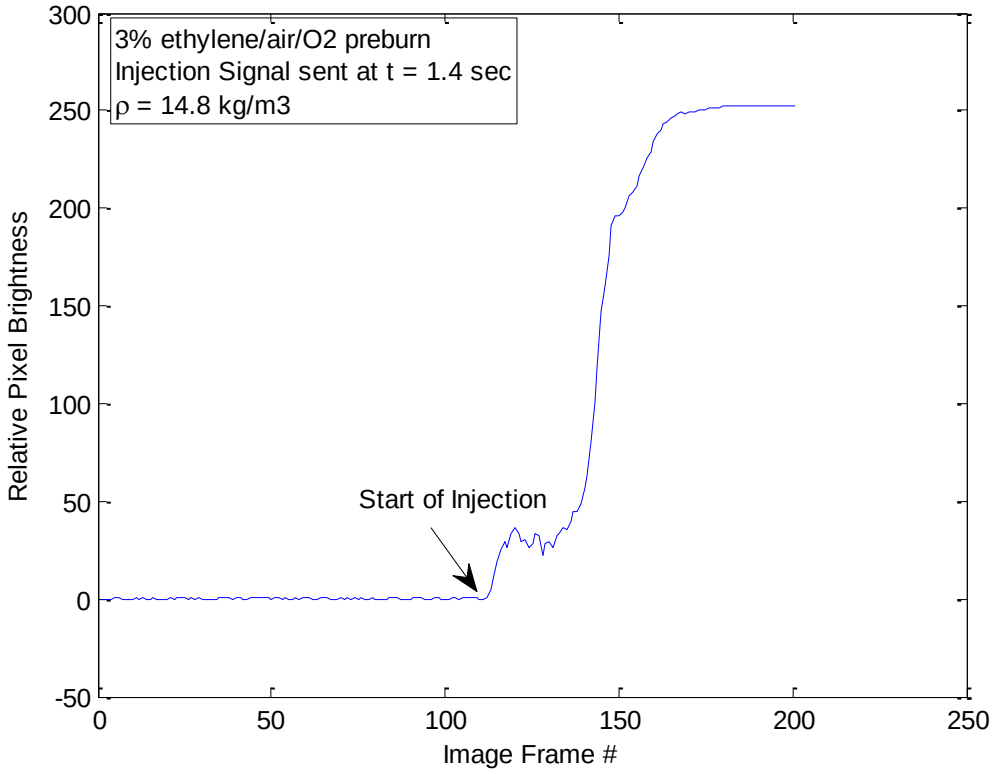

Figure 27 Start of injection (SOI) processed pixel average

b. Start of Combustion

Differing from the definition of SOI, start of combustion was not as easily defined. Two definitions could be used: 1) start of combustion could be defined to be the instant that the first molecule of fuel initially appeared to combust, or 2) start of combustion could be defined to be the instant that the bulk section of the fuel began to combust. Figure 28 shows the typical ignition sequence for the Yanmar injector. Because the fuel was dyed, the entire injector spray can be seen in the high speed images, the star

pattern shape is the fuel as it sprays out of the injector. The increased intensity of light along the fuel jets in the images relates to the occurrence of combustion.

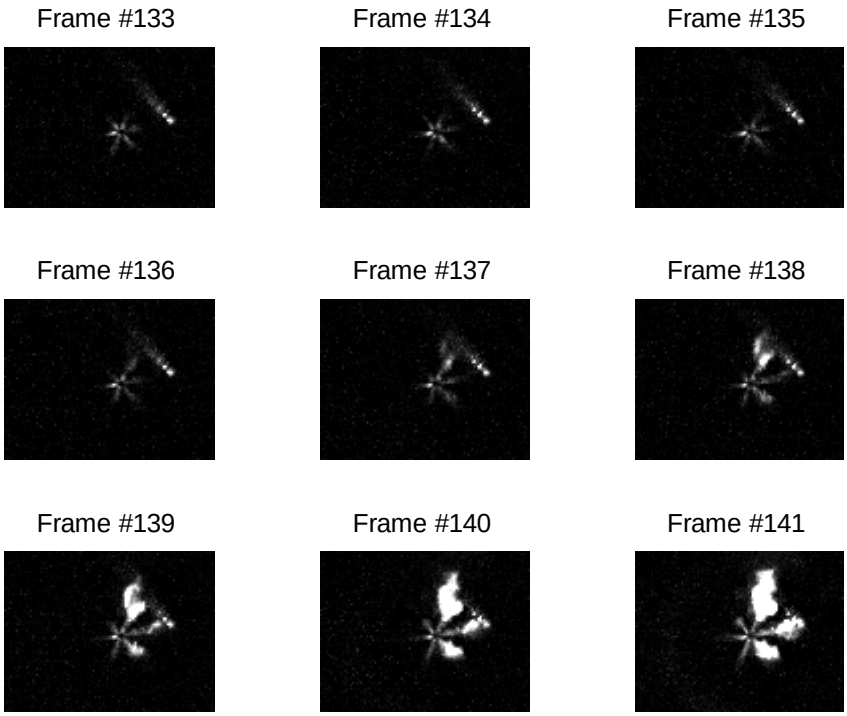

Figure 28 Start of combustion sequence

Appendix C contains the code used to determine the start of combustion based on the first definition, the first occurrence of combustion. Similar to the determination of SOI, this code found the maximum pixel value for each frame, and determined the frame at which that value significantly increased. This approach proved less robust at yielding consistent results throughout the testing. The laser reflection on the optical window, evidenced as the streak in the top right corner of each image in Figure 28, needed to be removed from the image, and thus any combustion occurring in that area could not be considered in the analysis. Also, the average pixel value varied with a certain amount of noise, and required a thresholding method to determine when the spike occurred, which is

a similar technique as the bulk averaging method. This method was explored as a means to calculate SOC, but was not used in this study.

Appendix D contains the code used to determine the start of combustion based on the second definition, the first occurrence of bulk combustion. This code operated similar to that used to determine SOI, using an averaging approach. The value of each pixel in the frame was averaged and bulk combustion was determined to be the frame when this average began to increase. Figure 29 shows the a typical plot for the average pixel value in each frame. The code determined that this value occurred at Frame 136, which corresponds with the initial appearance of combustion visually in Figure 28.

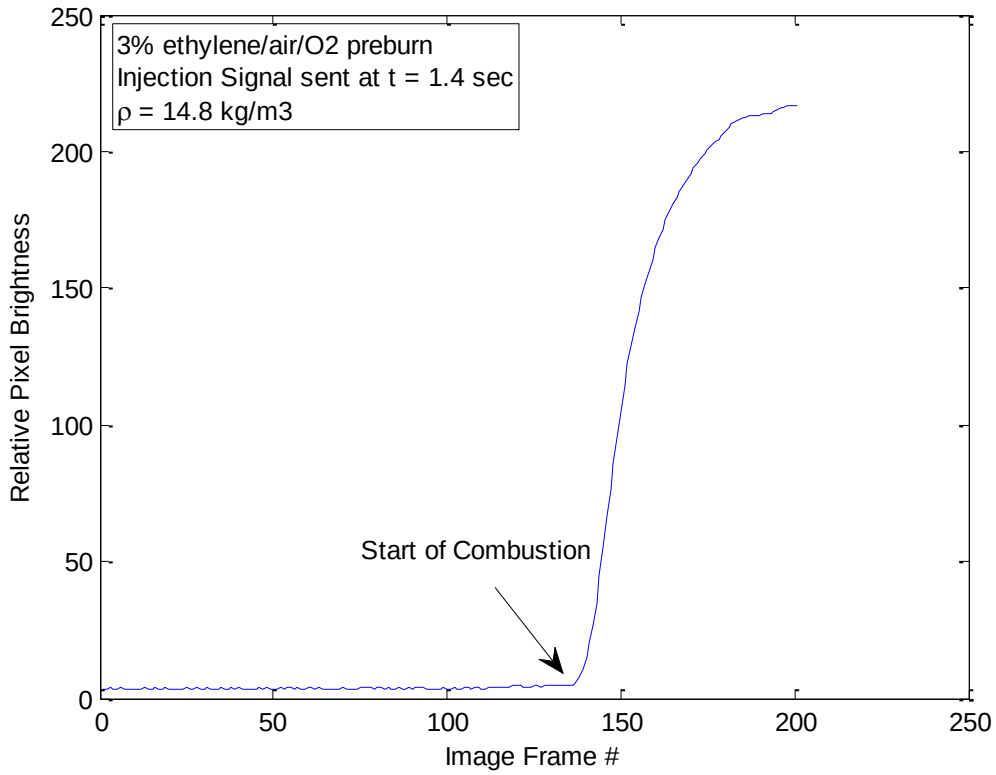

Figure 29 Start of combustion processed pixel maximum

Compared with the first definition, using the initial onset of combustion to determine SOC, the bulk combustion approach resulted in SOC that always occurred later; however, the bulk combustion approach was used as the primary means of

determining start of combustion because it corresponds with techniques used by other researches in the field. As mentioned in the introduction, researchers have been using pressure to determine when ignition begins, which itself is a bulk measurement. Also, the bulk averaging of the frame decreases the effect that outliers, quickly combusting fuel droplets, would have on the determination of the start of combustion. The time at start of combustion was determined from the time stamp of the frame where the code indicated bulk combustion began.

c. Alternative Methods for Determining Start of Injection

In addition to using the high speed imaging, two different methods for determining the time of SOI were also explored during this experiment. The high speed imaging is dependent on being able to maintain a clear image through the optical window throughout the test. As mentioned previously, the combustion products from the preburn are primarily water and carbon dioxide. The fuel injection event and subsequent combustion could potentially produce soot which would occlude the window. Once occluded, additional imaging data could not be taken for hours, sufficient time was required to allow the walls to cool, clean the window, and then reheat the walls. Initially, it was thought that the time delay between the trigger signal that initiated the injection sequence and the actual injection of the fuel into the chamber would be a repeatable value that could be used to determine start of injection. This delay was determined by running "cold tests," runs where the preburn was not initiated, and taking data using the high speed imaging system. The lack of any combustion in these cold runs eliminated the possibility of the optical window being occluded, and the high speed images were consistently clear. Table 4 shows the statistical results for the cold tests. These data show that the time interval between the injection trigger and the start of injection was not consistent. The standard deviation for a given pressure ranges from 1.16 to 3.06 milliseconds. The magnitude of the ID being studied in this project is on the same order as the magnitude of the error using this method, and thus this method would not be effective at determining SOI. The data also shows that the performance of the injector did not significantly increase for a specific pressure.

Table 4 Trigger-SOI delay statistics

Pressure (psi)	Runs (# total)	SOI Delay (msec)	Std. Deviation (msec)
3600	7	58.66	2.33
3750	6	58.15	2.83
3850	5	60.16	2.86
4000	5	57.02	2.24
4100	5	59.14	2.91
4250	5	57.62	1.16
4350	5	59.32	3.06
4500	7	59.43	2.00

Based on the testing apparatus set up for the Yanmar injector, it was thought that the inconsistency in the data resulted from the actuation of the high speed valve which received the injection trigger then opened the valve that delivered the high pressure fuel to the injector. A high speed Kistler pressure gage, similar to the gage used to measure the dynamic pressure in the chamber, was added to the fuel line after the high speed gage and before the Yanmar injector. The cold runs were conducted again in the same manner as described previously, in an attempt to find a constant time delay between the high pressure fuel being delivered to the injector and the actual start of injection. Table 5 shows the results from these runs. It is clear that again, there was no consistent delay. The variation in the data is greater than what was desired for the experiment, and thus this method was not used. These tests determined that the time required for the Yanmar injector to actuate, measured from the arrival of high pressure fluid to the fuel spray leaving the injector tip, was not consistent in each run, and varied on the order of hundreds of microseconds.

Table 5 Delivery of pressurized fuel to SOI delay statistics

Pressure (psi)	Runs (# total)	Actuation Delay (msec)	Std. Deviation (msec)
3500	3	5.48	0.12
3750	4	5.40	0.45
4000	2	5.30	0.00
4150	4	5.34	0.46

After this analysis, it was determined that the high speed imaging system produced the most consistent and accurate results with the least amount of variation. This method was used as the primary means of determining the time at which start of injection occurred. It was imperative that the optical window remain clean throughout the combustion events for this data to be taken, and steps were developed to ensure that the window remain clean.

B. AVERAGE PREBURN TEMPERATURE PLOTS

Table 6 shows the test cases used to determine the statistical temperature behavior for SOI for the testing. The lower density condition, ρ = 7.65 kg/m^3, corresponds to an engine compression ratio of approximately 6.35:1, while the higher density condition, ρ = 14.8 kg/m^3, corresponds to an engine compression ratio of approximately 12.3:1. These compression ratios represent the lower end of Navy-relevant diesel engines.

Table 6 Test case summary for preburn characterization

Density (kg/m^3)	Preburn (% ethylene)	# of runs
7.65	3	4
7.65	2	5
14.8	3	1
14.8	2	5

As shown in the table, the characterization of the chamber for the 14.8 kg/m^3, 3% ethylene preburn mixture were only based off the results of a single run. The chamber preburn reaction was violent enough that the ceramic sheathe protecting the

thermocouples was fractured, and caused failure in the thermocouple. Ten different thermocouples were used in an attempt to gather more data for this condition, but only a single run provided meaningful results; however, this condition was measured using a larger gage thermocouple, a protected 0.005 in. sheathed in a metal tube instead of the 0.003 in. sheathed in a ceramic, and the results agreed with those determined by the single run with the smaller thermocouple. Based on this, it is assumed that the temperature plot has been accurately determined. The variability for the SOI temperature for each individual ID test run was calculated to be the standard deviation of the aggregate preburn runs for that given temperature. Because the error for the other three cases was similar, it is assumed that the error for the 14.8 kg/m^3, 3% ethylene condition had the same uncertainty as the 14.8 kg/m^3, 2% ethylene preburn condition.

Figure 30 and Figure 31 show the results for the average preburn runs for the four different testing conditions. The temperature for the 3% ethylene preburns, regardless of density, peaked at approximately 1600 K, while the temperature for the 2% ethylene preburns peaked at approximately 1400 K. The plots show that for the higher density runs, the temperature decreased at a slower rate. The higher preburn density remained above 800 K for the entire four seconds of recorded data, while the lower density cases dipped below 800 K for the same time period.

Differing from the temperature response, the figures show that the pressure peak varied significantly depending on the chamber density. For the high density condition, the pressure peaked at approximately 9.1 MPa and 6.5 MPa for the 3% and 2% preburns, respectively, while at the lower density testing condition, the pressure peaked at approximately 4.3 MPa and 3.3 MPa.

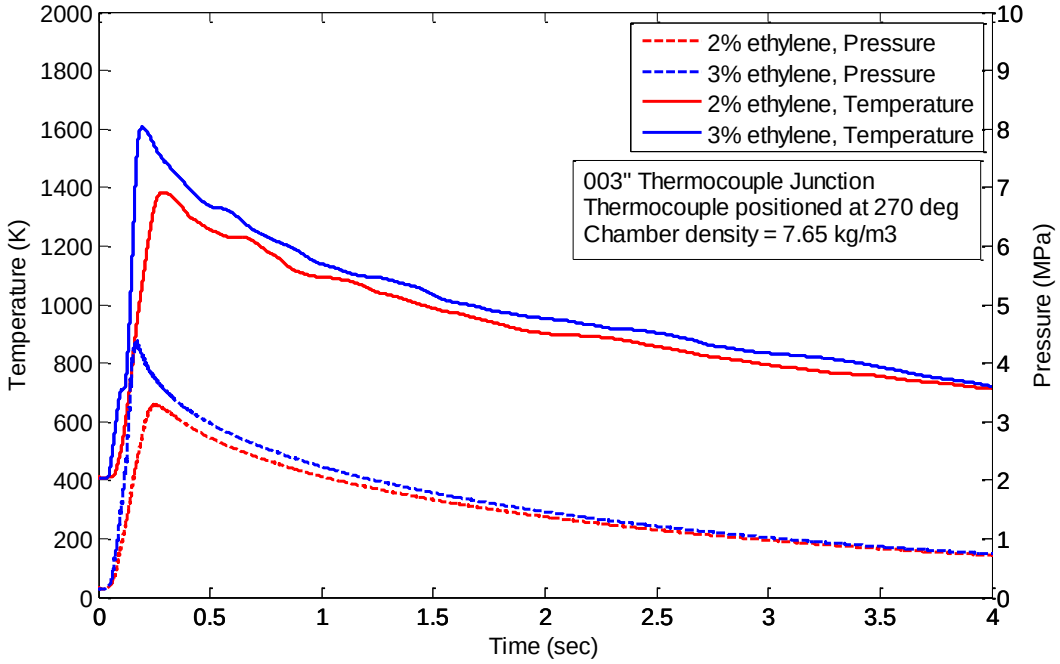

Figure 30 Average preburn temperature and pressure plot for ρ = 7.65 kg/m^3,

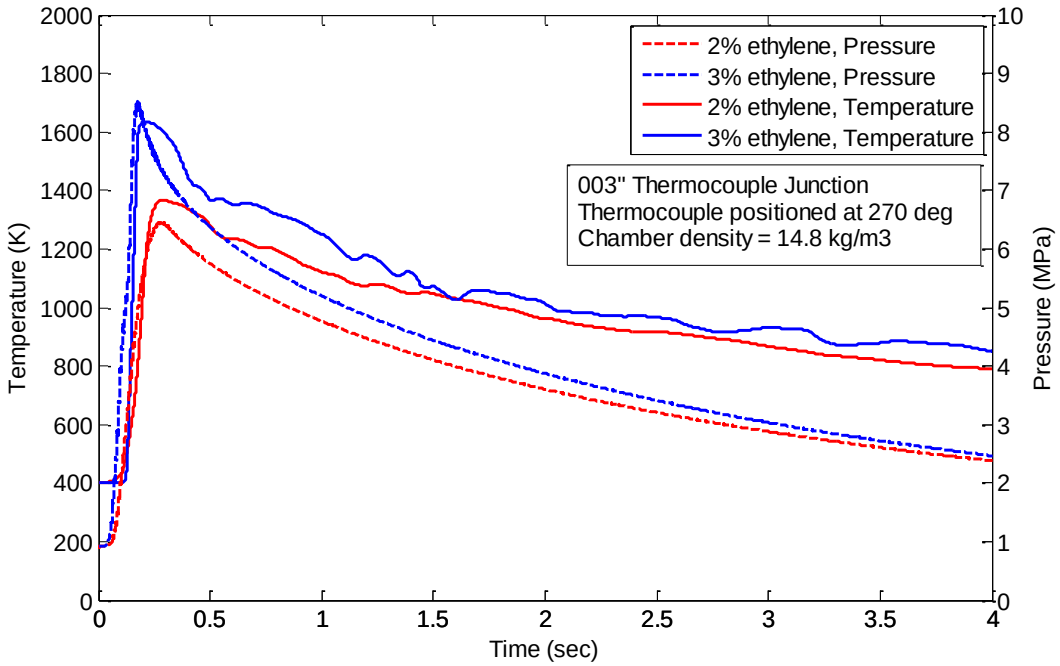

Figure 31 Average preburn temperature and pressure plot for ρ = 14.8 kg/m^3,

C. YANMAR RESULTS

1. Yanmar Injector, $\rho = 7.65$ kg/m^3

a. Test Case Summary

Table 7 shows the test case summary for the Yanmar injector, at the given operating conditions. For each given set of conditions, the average ID was determined using by taking an average of all the runs taken. The error in the ID determination was found from the standard deviation of the runs taken under specific conditions.

Table 7 Test case summary for the Yanmar injector, $\rho = 7.65$ kg/m^3

Yanmar Injector, $\rho = 7.65$ kg/m^3		
Injection Trigger Delay (sec)	**Preburn (% ethylene)**	**# of runs**
0.8	3%	4
1.0	3%	3
1.2	3%	3
1.4	3%	4
1.4	2%	3
1.5	2%	5

b. ID versus Injection Temperature Results

The results for the low density, Yanmar injector tests are shown in Figure 32. The figure shows that for the testing conditions, there is little difference between the F-76 and the F-76/HRD blend fuel. The DSH fuel appears to demonstrate high to changes in the injection temperature, combusting slightly quicker at high temperatures and slightly slower when compared to the other fuels at lower temperatures.

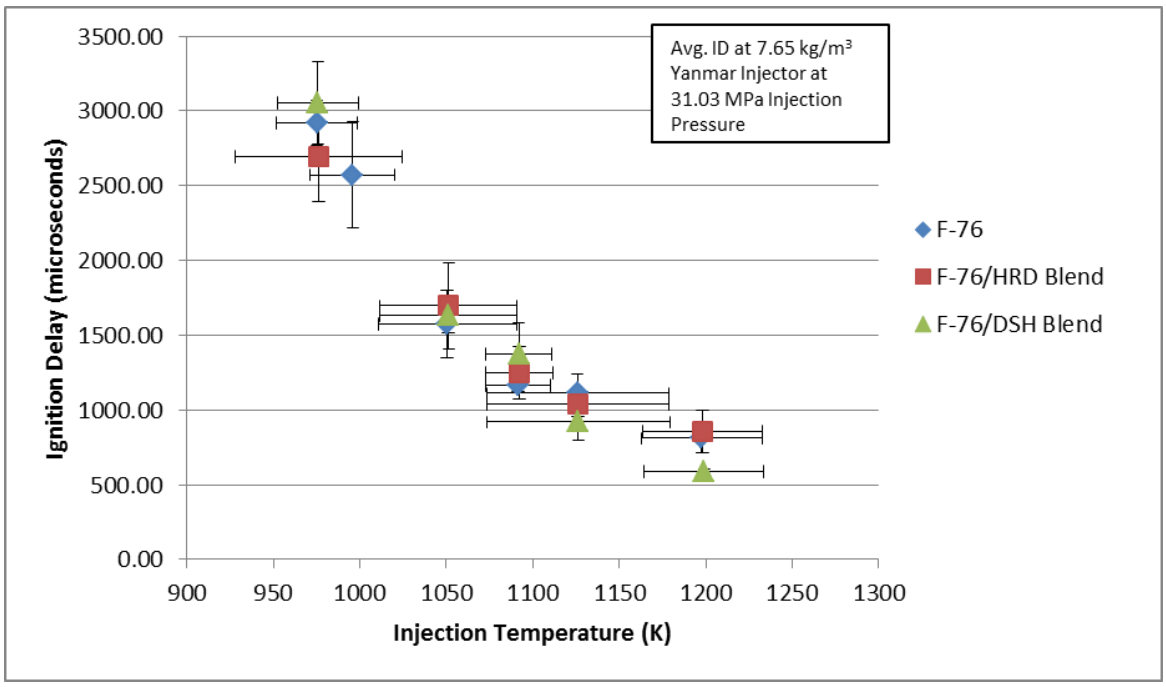

Figure 32 Yanmar injector results, ρ = 7.65 kg/m^3

2. Yanmar Injector, ρ = 14.8 kg/m^3

a. Test Case Summary

Table 8 shows the test case summary for the Yanmar injector at the higher density. The ID and error was determined using the same method as at the lower density. Data was collected at additional injection temperatures (injection trigger delay) in an attempt to increase the resolution of the ID profile.

Table 8 Test case summary for the Yanmar injector, ρ = 14.8 kg/m^3

Yanmar Injector, ρ = 14.8 kg/m^3		
Injection Trigger Delay (sec)	**Preburn (% ethylene)**	**# of runs**
0.8	3%	4
1.0	3%	4
1.2	3%	3
1.4	3%	3
1.5	3%	1
1.35	2%	2
1.5	2%	3

b. ID versus Injection Temperature Results

Figure 33 shows the results for the Yanmar injector using the high-density conditions. The DSH fuel was not tested at these conditions. The figure shows that the F-76 and the F-76/HRD blend have very similar ID, and that the two fuels generally follow the same trend.

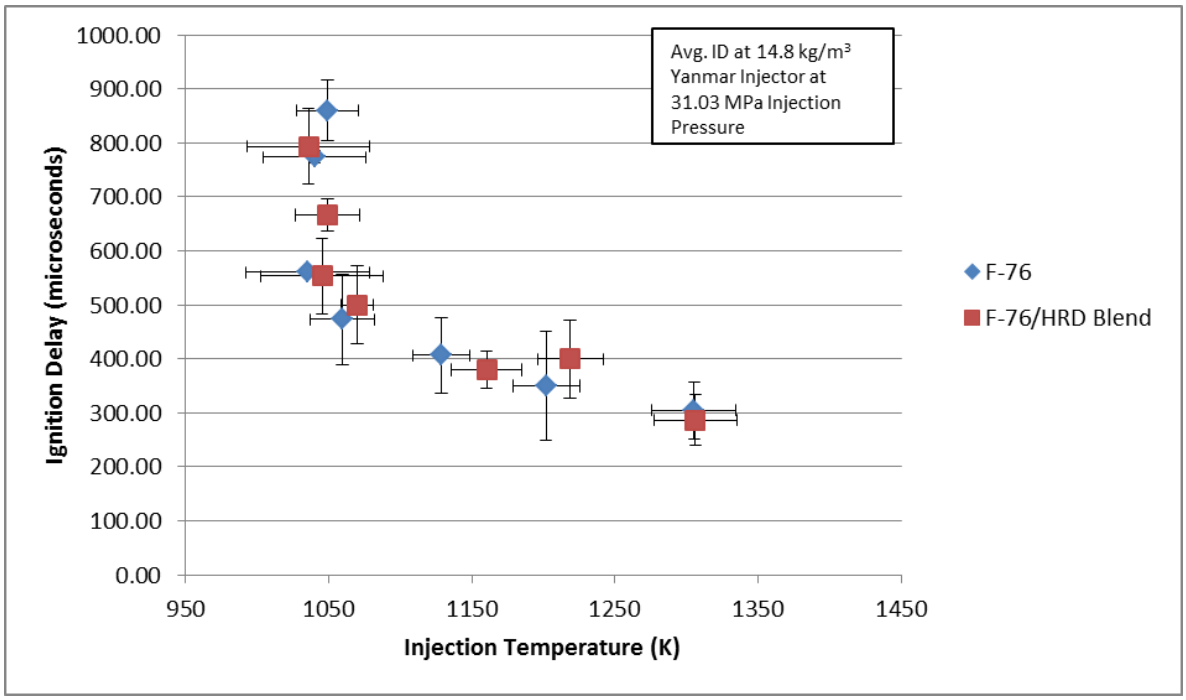

Figure 33 Yanmar injector results, ρ = 14.8 kg/m^3

Figure 34 shows the results from the high and low density test cases on the same axes. As expected, the higher density injection conditions resulted in a smaller ID, for the same temperature and also decreased the effect of the change in temperature.

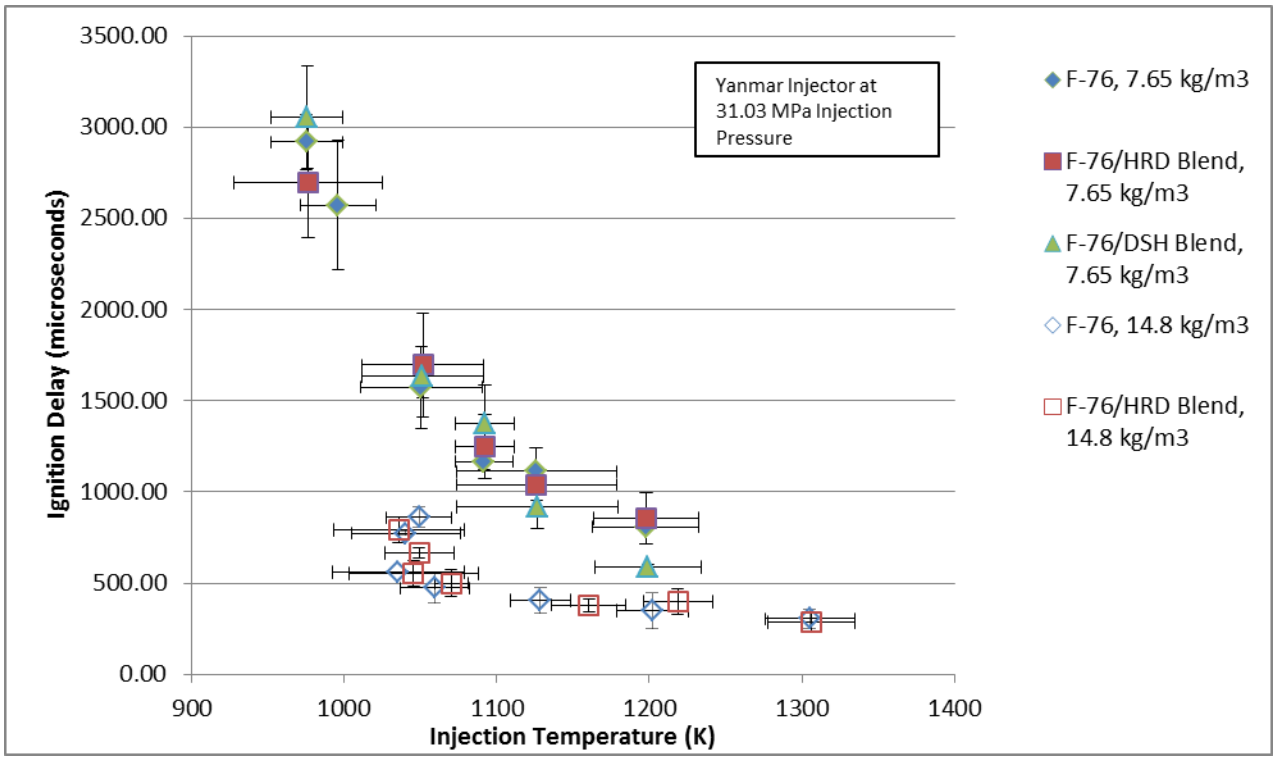

Figure 34 Yanmar injector results

D. EMD RESULTS

1. Test Case Summary

Table 9 shows the test case summary for the EMD injector. Data was only collected at the higher density operating conditions for this injector, as the lower density, with a compression ratio of approx. 6.35:1, is not relevant to the practical operation of the EMD injector. The experimental procedure and material performance of the testing apparatus was more deeply understood during the latter experimental tests and thus the data collection is more uniform for the EMD than the Yanmar injector. The ID and error were determined in the same manner as for the Yanmar injector.

Table 9 Test case summary for the EMD injector, ρ = 14.8 kg/m^3

EMD Injector, ρ = 14.8 kg/m^3		
Injection Trigger Delay (sec)	**Preburn (% ethylene)**	**# of runs**
0.8	3%	3
1.0	3%	3
1.2	3%	3
1.4	3%	3
1.5	3%	3
1.35	2%	3
1.5	2%	3

2. ID vs. Injection Temperature Results, optical emission measurements

Figure 35 shows the results for the F-76 and F-76/HRD blends being injected from EMD injector. Consistent with the high-density Yanmar results, the two fuels performed very similar throughout the EMD injections. As lower injection temperatures were reached, T ~ 1100 K, the F-76/HRD blend fuel does ignite slightly quicker than the F-76 fuel.

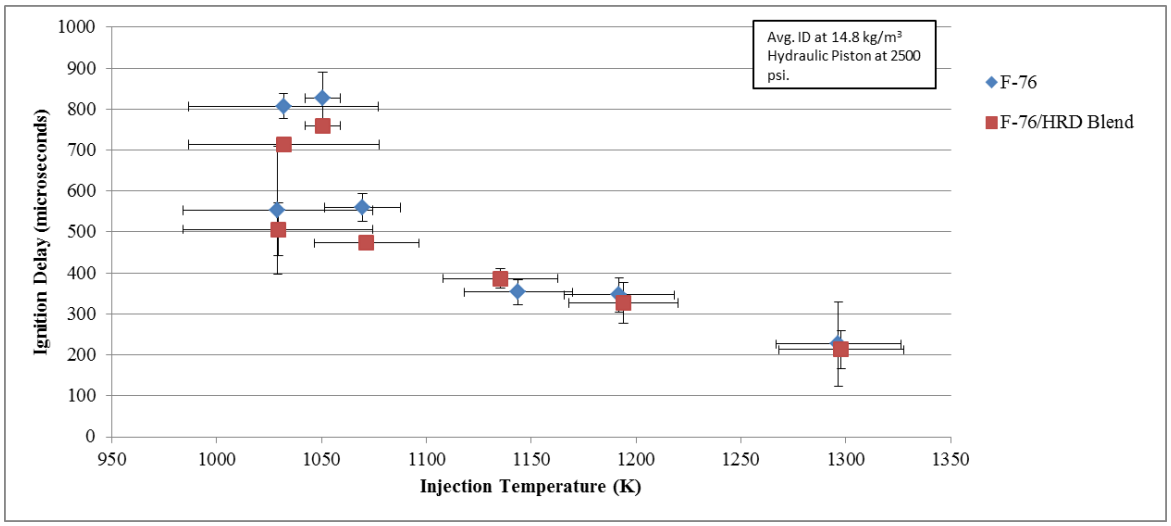

Figure 35 EMD ID versus injection temperature results

It is important to note the ID trends shown on the Yanmar and EMD high density plots, Figure 33 and Figure 35, show a type of incongruence at the lower end of temperatures tested. The ID values appear to stack on top of each other in the 1000 K to 1100 K injection temperature range. The cases at with the longer ID were conducted with a 2% ethylene preburn while the cases with the shorter ID were conducted with a 3% preburn. Although the temperatures at start of injection ended up being equal, the pressure at this point different. As shown in previously in Equation (2), ID is dependent not only on temperature but also on pressure. The data in Table 10 show that the total pressure at SOI was different between two runs where all conditions were held the same other than the % ethylene in the preburn mixture. The table shows that although the injection temperature was nearly the same, the ID varied significantly due to the injection pressure differences.

Table 10 Preburn pressure comparison

EMD Injector, ρ = 14.8 kg/m^3				
Trigger Delay (sec)	**Preburn Mixture (%ethylene)**	**Avg Injection Temperature (K)**	**Avg Injection Pressure (MPa)**	**Avg ID (μsec)**
1.5	3	1029.3	4.53	507.00
1.5	2	1031.9	4.29	713.00

THIS PAGE INTENTIONALLY LEFT BLANK

IV. CONCLUSIONS AND FUTURE WORK

A. CONCLUSIONS

Based on the ignition delay results, the F-76/HRD 50/50 blend exhibits drop-in compatibility with conventional F-76 diesel fuel when operated with a Yanmar or an EMD injector. The two fuels performed nearly exactly the same throughout the testing; however, for the high density, low temperature injection cases, the F-76/HRD blend fuel began to behave differently, having a ID that trended slightly faster than the F-76 case. This is most likely due to the difference in cetane number between the two fuels. At the lower temperatures, the longer, paraffinic chains in the HRD fuel combusted at a faster rate than the more complex, conventional diesel fuel. It is expected that as the temperature continues to decrease, the ignition properties of the two fuels would continue to diverge. Although the fuel is slightly more sensitive to injection temperature variations, the F-76/DSH 50/50 blend exhibits drop-in compatibility with conventional F-76 diesel fuel for the Yanmar injector at low densities.

B. FUTURE WORK

In order to more fully characterize the ID performance of the test fuels, the experimental conditions could be varied. Higher testing densities could be used to determine the fuel performance for engines with higher compression ratios. Additionally, lower SOI temperatures could be tested in order to find the performance of the fuels for engines running at lower speeds, such as idling. These experiments could be conducted using the existing testing apparatus, so long as the preburn and injection pressures do not exceed the material limits of the combustion chamber.

More work could also be done to improve the determination of temperature at SOI. Using the same testing apparatus, additional samples could be taken at each of the testing conditions to determine a more accurate average temperature plot, as well as more thoroughly calculate the expected error. Another viable method of determining the temperature at SOI would be taking thermocouple readings for each injection run. This method was attempted throughout this study, but the thermocouples were not able to

consistently capture the temperature. Improvements to the thermocouple preparation could be applied, or different thermocouples entirely could be used.

Similar to improving the determination of SOI temperature, the average ID and expected error for the fuels at the given testing conditions could be improved by taking more samples at each condition; however, the results published in this research, along with the error determinations shown in the plots, are sufficient to characterize the ID performance of the fuels and injectors tested.

As the Navy moves forward in the qualification of alternative fuels for its platforms, this testing procedure is applicable and relevant. Different fuels could be tested using the Yanmar and EMD injectors, or different injectors could be added to the testing apparatus.

APPENDIX A. ENGINEERING DRAWINGS

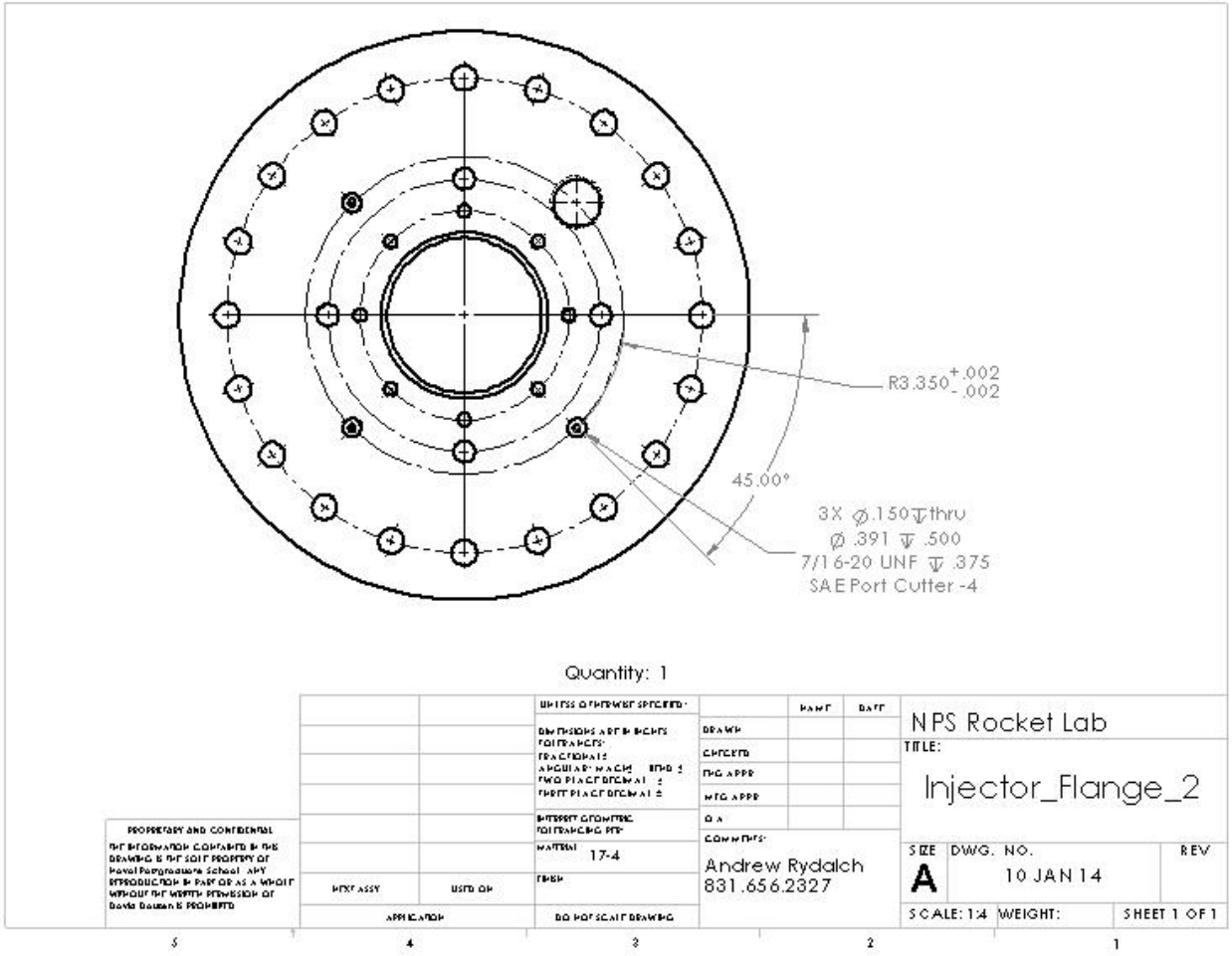

THIS PAGE INTENTIONALLY LEFT BLANK

APPENDIX B. START OF INJECTION

```
%Created By Dave Dausen and Andrew Rydalch
%
%Program to read high speed Imaging and calculate the Start of Injection.  This
%  work will also infer the Start of Ignition as well if the intensities are
%  high enough to accuratley detect.

%Imaging is done using the SA5 where Framerate is 50000 frames per second.
%  Pixel size is not specified.

clc
clear all
close all

format long

date = '12';    %Date tests were conducted
N = 22;         %Number of tests conducted that day

for i = 1:N

% Import the images from each test
filename = ['EMD_Injection' num2str(date) 'MayRun' num2str(i) '_C001H001S0001.avi'];
MovieOrig = VideoReader(filename);  % *.avi name

Frames = MovieOrig.NumberOfFrames;
FramesRate = MovieOrig.FrameRate;
PictureHeight = MovieOrig.Height;
PictureWidth = MovieOrig.Width;

% User inputs
OrigFrameRate = 50000;      %Framerate of imaging system
% Computer time at which image data began
InitialTime = [0.899 0.899 0.877 0.880 ...
    1.089 1.0875 1.094 ...
    1.293 1.291 1.297 ...
    1.496 1.507 1.500 ...
    1.582 1.582 1.585 ...
    1.581 1.587 1.589 ...
    1.440 1.440 1.442];  %seconds
FrameDelta = 1/OrigFrameRate;  %Time between freames, seconds
InjectionBox = [325 128 15 15]; %Box around injector tip for SOI
StartInjThresh = 8;  %Threshhold for Start of Injection (Averaged)

% Preallocate movie structure.
MovieOrigStructure(1:Frames) = ...
    struct('Picturedata', zeros(PictureHeight, PictureWidth, 3, 'uint8'),...
           'colormap', []);
```

```
% Read one frame at a time into structure.
for F = 1:Frames
    MovieOrigStructure(F).Picturedata = read(MovieOrig, F);
end

% Preallocate variable space
ImageInjAvg = zeros(Frames,1);

%Proccess the first intial 100 frames to determine background and average.
for F = 1:Frames
    %Open the original movie frame by frame recognizing common data in a
    %  disk with radius of 1 pixels and N periodic line structure elements.
    %  Only look at every 4 frames to avoid double counting of particles.
    %This can be modified based on sensitivity.
    Image = imopen(MovieOrigStructure(F).Picturedata, strel('arbitrary',1));

    %Crop the image to only look in the Injection box
    ImageInjInjection = imcrop(Image, InjectionBox);

    %Average Value for cropped image
    ImageInjAvg(F) = mean2(ImageInjInjection(:,:,1));
end

%Find the average background noise
ImageInjBackground = mean(ImageInjAvg(1:20,1));
%Remove the average background noise
ImageInjProcessed = ImageInjAvg - ImageInjBackground;

% Apply the threshold to determine SOI
F = 1;
while floor(ImageInjProcessed(F)*10) + floor(ImageInjProcessed(F+1)*10) <=
2*StartInjThresh
    F = F + 1;
end

%Frame where the injection starts
InjectionStartFrame(i) = F;

%Computing the start of injection in time
StartInjection(i,1) = ((InjectionStartFrame(i) - 1) * FrameDelta) + InitialTime(i);
end
```

Published with MATLAB® R2012b

APPENDIX C. START OF COMBUSTION, MAXIMUM VALUE

```
%Dave Dausen and Andrew Rydalch
%
%Program to read high speed Imaging and calculate the Start of Injection.  This
%  work will also infer the Start of Ignition as well if the intensities are
%  high enough to accuratley detect.

%Imaging is done using the SA5 where Framerate is 50000 frames per second.
%  Pixel size is not specified.

clc
clear all
close all

format long

date = 26   %Date tests were conducted
N = 21;     %Number of tests conducted that day

for i = 1:N

% Import the images from each test
filename = ['EMD_Injection' num2str(date) 'MayRun' num2str(i) '_C001H001S0001.avi'];
MovieOrig = VideoReader(filename);  % *.avi name

Frames = MovieOrig.NumberOfFrames;
FramesRate = MovieOrig.FrameRate;
PictureHeight = MovieOrig.Height;
PictureWidth = MovieOrig.Width;

% User inputs
OrigFrameRate = 50000;      %Framerate of imaging system
% Computer time at which image data began
InitialTime = [1.0558 1.0546 1.05600 1.056 1.059];  %seconds
FrameDelta = 1/OrigFrameRate;   %Time between freames, seconds
IgnitionBox = [160 20 300 230]; % Crop out the edges of the image
StartIgnThresh = 2000;  % Threshhold for Start of Ignition (Maximum)

% Preallocate movie structure.
MovieOrigStructure(1:Frames) = ...
    struct('Picturedata', zeros(PictureHeight, PictureWidth, 3, 'uint8'),...
           'colormap', []);

% Read one frame at a time into structure.
for F = 1:Frames
    MovieOrigStructure(F).Picturedata = read(MovieOrig, F);
end
```

```
% Preallocate variable space
ImageIgnMax = zeros(Frames,1);


%Proccess the first intial 100 frames to determine background and average.
for F = 1:Frames
    %Open the original movie frame by frame recognizing common data in a
    %  disk with radius of 1 pixels and N periodic line structure elements.
    %  Only look at every 4 frames to avoid double counting of particles.
    %This can be modified based on sensitivity.
    Image = imopen(MovieOrigStructure(F).Picturedata, strel('arbitrary',1));

    %Crop out the laser reflection image
    Image(90:138,389:630,:) = 0;

    %Crop out the edges
    ImageInjIgnition = imcrop(Image, IgnitionBox);

    %Maximum Value of Larger Cropped Image to see ignition onset
    [ImageIgnMax(F),IgnIndex] = max(max(ImageInjIgnition(:,:,1)));
end

%Find the average background noise
ImageIgnBackground = mean(ImageIgnMax(1:20,1));
%Remove the average background noise
ImageIgnProcessed = ImageIgnMax - ImageIgnBackground;

% Apply the threshold to determine SOC
while floor(sum(ImageIgnProcessed(F:F+5))*100) <=  6*StartIgnThresh
    F = F + 1;
end

%Frame where the ignition starts
IgnitionStartFrame(i) = F;

%Computing the start of combustion
StartIgnition(i) = ((IgnitionStartFrame(i) - 1) * FrameDelta) + InitialTime(i);
end
```

Published with MATLAB® R2012b

APPENDIX D. START OF COMBUSTION, BULK AVERAGE

```
%Dave Dausen and Andrew Rydalch
%
%Program to read high speed Imaging and calculate the Start of Injection.  This
%  work will also infer the Start of Ignition as well if the intensities are
%  high enough to accuratley detect.

%Imaging is done using the SA5 where Framerate is 50000 frames per second.
%  Pixel size is not specified.

clc
clear all
close all

format long

date = '12';
N = 22;

for i = 1:N

% Import the images from each test
filename = ['EMD_Injection' num2str(date) 'MayRun' num2str(i) '_C001H001S0001.avi'];
MovieOrig = VideoReader(filename);  % *.avi name

Frames = MovieOrig.NumberOfFrames;
FramesRate = MovieOrig.FrameRate;
PictureHeight = MovieOrig.Height;
PictureWidth = MovieOrig.Width;

% User inputs
OrigFrameRate = 50000;      %Framerate of imaging system
% Computer time at which image data began
InitialTime = [0.899 0.899 0.877 0.880 ...
    1.089 1.0875 1.094 ...
    1.293 1.291 1.297 ...
    1.496 1.507 1.500 ...
    1.582 1.582 1.585 ...
    1.581 1.587 1.589 ...
    1.440 1.440 1.442];  %seconds
FrameDelta = 1/OrigFrameRate;   %Time between freames, seconds
IgnitionBox = [160 20 300 230]; % Crop out the edges of the image
StartIgnThresh = 2000;  % Threshhold for Start of Ignition (Maximum)

% Preallocate movie structure.
MovieOrigStructure(1:Frames) = ...
    struct('Picturedata', zeros(PictureHeight, PictureWidth, 3, 'uint8'),...
           'colormap', []);
```

```
% Read one frame at a time into structure.
for F = 1:Frames
    MovieOrigStructure(F).Picturedata = read(MovieOrig, F);
end

% Preallocate variable space
ImageIgnAvg = zeros(Frames,1);

%Proccess the first intial 100 frames to determine background and average.
for F = 1:Frames
    %Open the original movie frame by frame recognizing common data in a
    %  disk with radius of 1 pixels and N periodic line structure elements.
    %  Only look at every 4 frames to avoid double counting of particles.
    %This can be modified based on sensitivity.
    Image = imopen(MovieOrigStructure(F).Picturedata, strel('arbitrary',1));

    %Crop out the edges
    ImageInjIgnition = imcrop(Image, IgnitionBox);

    %Average Value for Cropped Image
    ImageInjAvg(F) = mean2(ImageInjInjection(:,:,1));
end

%Find the average background noise
ImageIgnBackground_2 = mean(ImageIgnAvg(1:20,1));
%Remove the average background noise
ImageIgnProcessed_2 = ImageIgnAvg - ImageIgnBackground_2;

% Apply the threshold to determine SOC
while floor(sum(ImageIgnProcessed_2(F:F+5))*100) <=  6*StartIgnThresh
    F = F + 1;
end

%Frame where the ignition starts
IgnitionStartFrame(i) = F;

%Computing the start of combustion
StartIgnition(i,1) = ((IgnitionStartFrame(i) - 1) * FrameDelta) + InitialTime(i);
end
```

Published with MATLAB® R2012b

LIST OF REFERENCES

[1] A. M. Chambers and S. A. Yetiv, "The Great Green Fleet: The U.S. Navy and fossil-fuel alternatives," *Naval War College Review*, vol. 64, no. 3, pp. 61–77, Summer-2011.

[2] U.S. Energy Information Administration. (2011, May 25). "U.S. oil import dependence: Declining no matter how you measure it," *This Week in Petroleum* [Online]. Available: http://www.eia.gov/oog/info/twip/twiparch/2011/110525/twipprint.html

[3] L. Daniel. (2010, July 22). "New office aims to reduce military's fuel usage," *American Forces Press Service* [Online]. Available: http://www.defense.gov/News/NewsArticle.aspx?ID=60131

[4] R. Mabus (2009 Oct. 14). Remarks by the Honorable Ray Mabus presented at *Naval Energy Forum* [Online]. Available: http://www.navy.mil/navydata/people/secnav/Mabus/Speech/SECNAV%20Energy%20Forum%2014%20Oct%2009%20Rel1.pdf

[5] S. Ghosh and T. Risley, "Alternative fuel for marine application," U.S. Maritime Administration, Pittsburgh, PA, Final Rep. G0004.EHP6.058, Feb. 2012.

[6] A. D. Stein. (2012, Aug. 31). "NPS researchers evaluate biofuels for powering the fleet," America's Navy [Online]. Available: http://www.navy.mil/submit/display.asp?story_id=69357

[7] L. Poirier. (2011 Mar.). "Enabling the Navy's Great Green Fleet," Hart Energy [Online]. Available: http://www.hartfuel.com/2011_03/Enabling-the-Navs-Great-Green-Fleet.php

[8] W. P. Fischer, "Design and qualification of a high-pressure combustion chamber for ignition delay testing of diesel fuels," M.S. thesis, MAE, NPS, Monterey, CA, 2013.

[9] Oilgae. (2013 Jan.). "Algae oil information," [Online]. Available: http://www.oilgae.com/algae/oil/oil.html

[10] P. Y. Hsieh, J. A. Widegren, T. J. Fortin, and T. J. Bruno, "Chemical and thermophysical characterization of an algae-based hydrotreated renewable diesel fuel." *Energy Fuels*, vol. 28, no. 5, pp. 3192–3205, Apr. 2014.

[11] M. Kazuhisa, "Renewable biological systems for alternative sustainable energy production," FAO, Rome, Italy, Bul. 128, 1997.

[12] Naval Technology. (2012 Jul. 19). “The U.S. Navy’s biofuel dilemma—Great Green Fleet sails into controversy” [Online]. Available: http://www.naval-technology.com/features/featurerimpac-us-navy-biofuel-great-green-fleet/

[13] V. Koundinya. (2009 Jan.). “Corn Stover,” Agricultural Marketing Resource Center [Online]. Available: http://www.agmrc.org/renewable_energy/corn-stover.

[14] R. Davis, M. Biddy, E. Tan, L. Tao, and S. Jones, “Biological conversion of sugars to hydrocarbons technology pathway,” National Renewable Energy Laboratory, Golden, CO, Tech. Rep. NREL/TP-5100-58054, Mar. 2013.

[15] S. Woolard, “Reporting of defects and non-compliance,” U.S. Nuclear Regulatory Commission, Washington, DC, Tech. Report. 10CFR21-0109, May 2013.

[16] J. Khatry, “Thermodynamics and heat engines,” Hesston College [Online]. Available: http://www2.hesston.edu/Physics/Thermodynamics/heat.html

[17] M. J. Moran, H. N. Shapiro, D. D. Boettner, and M. B. Bailey, *Fundamentals of Engineering Thermodynamics*, 7th ed., Hoboken, NJ: John Wiley & Sons, 2011.

[18] J. B. Heywood, “Combustion in compression-ignition engines,” in *Internal Combustion Engine Fundamentals*, McGraw-Hill, 1988, pp. 517–539.

[19] E. F. Obert, *Internal Combustion Engines*, 2nd ed., Scranton, PA: International Textbook, 1950.

[20] K. K. Kuo, *Principles of Combustion*, 2nd ed., Hoboken, NJ: John Wiley & Sons, 2005.

[21] S. R. Turns, *An Introduction to Combustion: Concepts and Applications*, 3rd ed., New York, McGraw-Hill, 2011.

[22] J. H. Petersen, “Combustion heat release rate comparison of algae hydroprocessed renewable diesel to F-76 in a two-stroke diesel engine,” M.S. thesis, MAE, Naval Postgraduate School, Monterey, CA, 2013.

[23] L. M. Pickett, C. L. Genzale, G. Bruneaux, L.-M. Malbec, L. Hermant, C. Christiansen, and J. Schramm, “Comparison of diesel spray combustion in different high-temperature, high-pressure facilities,” *SAE Int. J. Engines*, vol. 3, no. 2, pp. 156–181, 2010.

[24] Clark Cooper, *Catalog No. EH-3.7, High Pressure Solenoid Valves*, Roebling, NJ: Clark Cooper, n.d.

[25] C. Pandy, “Characterization of detonation waves in an optically accessible rotating detonation engine,” M.S. thesis, MAE, Naval Postgraduate School., Monterey, CA, 2013.

THIS PAGE INTENTIONALLY LEFT BLANK

INITIAL DISTRIBUTION LIST

1. Defense Technical Information Center
   Ft. Belvoir, Virginia

2. Dudley Knox Library
   Naval Postgraduate School
   Monterey, California